Universitat Autònoma
de Barcelona

A thesis for the

Master in Telecommunications Engineering

Design considerations of a High-Q Tunable Coaxial Filter with single tuning element

Lluís Acosta Basagañas

lluis.acosta@e-campus.uab.cat

Supervisor: Pedro de Paco Sánchez

pedro.depaco@uab.cat

Department of Telecommunications and Systems Engineering

Universitat Autònoma de Barcelona (UAB)

Escola d'Enginyeria

July, 2020

El sotasignant, Pedro de Paco Sánchez, Professor de l'Escola Tècnica Superior d'Enginyeria (ETSE) de la Universitat Autònoma de Barcelona (UAB),

CERTIFICA:

Que el projecte presentat en aquesta memòria de Treball Final de Master ha estat realitzat sota la seva direcció per l'alumne Lluís Acosta Basagañas.

I, perquè consti a tots els efectes, signa el present certificat.

Bellaterra, 2 de Juliol de 2020.

Signatura: Pedro de Paco Sánchez

Resum:

En un món on els serveis de telecomunicació evolucionen constantment, la utilització de tecnologies reconfigurables veu un important creixement en la seva demanda. En el cas de filtres de radiofreqüència, parlem de filtres sintonitzables, tant en freqüència com en amplada de banda. Aquest tipus de filtres solen dependre de masses elements sintonitzadors, sent necessaris tants elements sintonitzadors com l'ordre del filtre a implementar.
Al llarg d'aquest treball s'estudia el disseny d'un filtre coaxial pasa-banda sintonitzable en freqüència presentat per primera vegada per Gowrish B. i R. Mansour, amb la particularitat que únicament depèn d'un element sintonitzador, independentment de l'ordre del filtre. Aquest filtre, basat en cavitats, és capaç de mantenir un alt rendiment en tot el rang de sintonització, mantenint sempre constant l'amplada de banda absoluta i baixes pèrdues.
Per a demostrar el comportament real del filtre, es fabrica un prototip de 4t ordre amb una amplada de banda relativa del 4% en tot el rang, aconseguint-se un rang de sintonització del 25%.

Resumen:

En un mundo donde los servicios de telecomunicación evolucionan constantemente, la utilización de tecnologías reconfigurables ve un importante crecimiento en su demanda. En el caso de filtros de radiofrecuencia, hablamos de filtros sintonizables, tanto en frecuencia como en ancho de banda. Este tipo de filtros suelen depender de demasiados elementos sintonizadores, siendo necesarios tantos elementos sintonizadores como el orden del filtro a implementar.
A lo largo de este trabajo se estudia el diseño de un filtro coaxial paso-banda sintonizable en frecuencia presentado por primera vez por Gowrish B. y R. Mansour, con la particularidad de que únicamente depende de un elemento sintonizador, independientemente del orden del filtro. Este filtro, basado en cavidades, es capaz de mantener un alto rendimiento en todo el rango de sintonización, manteniendo siempre constante el ancho de banda absoluto y bajas pérdidas.
Para demostrar el comportamiento real del filtro, se fabrica un prototipo de 4º orden con un ancho de banda relativo del 4% en todo el rango, consiguiéndose un rango de sintonización del 25%.

Summary:

In a world where telecommunication services continuously evolve, the demand of reconfigurable technologies increases. In the case of radiofrequency filters, we are speaking about tunable filters, even in frequency or bandwidth. Typically, this kind of filters depend on many tuning elements, being necessary a minimum number of tuning elements equal to the filter order to implement.
Throughout this thesis, a study of the design of a tunable coaxial passband filter presented for the first time by Gowrish B. and R. Mansour is carried out, with the particularity that only depends of a single tuning element, independently of the filter order. This filter, based in cavities, can maintain a high performance over the tuning range, exhibiting a constant bandwidth and low losses.
To demonstrate its actual behavior, a prototype of 4^{th} order is fabricated with a relative bandwidth of the 4% in the whole tuning range, achieving a tuning range of approximately 25%.

Contents

List of Figures

List of Tables

Chapter 1

Introduction

High performance RF tunable filters are needed in reconfigurable systems to facilitate efficient utilization of the available frequency spectrum. Nowadays, the increasing demand of telecommunication services forces the engineers to look for new strategies in order to co-exist with other services. Many applications, such as the new 5G mobile network, require a large number of filter banks on their receivers because of the several number of possible bands that a user might have. A possible way to optimize the physical implementation in such technologies might be the use of tunable filters.

Moreover, the possibility to adapt an existing network to a new generation makes worth the possibility to reuse filters by means of this tunability that they might have. Such deployments take place regularly when an operator has already installed a network, for example 4G, and wants to add the new generation, 5G. This leads to have an efficiently management of the hardware resources with a considerable save of cost at a medium/long term, and might let the operator focus on other new network requirements.

Installing wireless infrastructure equipment, that sometimes is difficult or impossible to access, such as a communication satellite or a remote radio unit (RRU) on top of a high communication tower, is a very costly task. By using tunable filters, one installation can serve many years using remote electronic tuning. If there is a need to change the frequency or bandwidth, the difficulty falls into a remote control. Satellites lifetime also experiments a growing because of the possibility to adapt to changing markets. This last scenario has already become significant as [3] explains and, for this reason, many satellite applications are requiring the use of reconfigurable technology such as tunable filters.

In general, they are in demand in front-end receivers for suppression of interfering signals and for relaxation of oscillator phase noise and requirements of dynamic range. Tunable filters have been proposed as well for high-power applications.

1.1 Motivation

The purpose of this project is to do an inverse engineering work of a High-Q tunable filter proposed in [2]. The key fact of this proposed filter is that a single tuning element controls the central band of the filter, irrespectively of the filter order. Typically, tunable filters require a number of elements equal to the filter order, however the elliptical proposed solution breaks with this topic with high performance. A 25 % tuning range is achieved keeping constant bandwidth and quality factor. The solution takes advantage of the shape of an elliptic cross-sectional waveguide where a half-wave coaxial resonator is placed.
We will try to understand and resolve the main considerations and methodologies hidden in the design steps of this filter, as well as understand the resonant structure itself.

When designing a RF component, the design engineer is given some requirements that the component must accomplish. These requirements usually come with a deadline of delivery. From this point, the design methodologies and steps followed obtain a big importance. Giving the right steps in time towards the final objective can be translated into a save of time that the engineer must always consider. For this reason, the understanding of the design methodologies followed in this project together with the fabrication of our own model can give us a view of which are the strategies to follow in designing microwaves components.

This proposed solution, and in general all three-dimensional (3D) filters, are focused on the satellites market. The possibility to contribute in a very strict and demanding market, as this one, mixed with the "simplicity" of the tuning mechanism makes the project even more interesting.
In a near future, thanks to the development of this thesis, we will be able to contribute in the research of this kind of structures of single tuning element.

1.2 Goals and structure of the thesis

After this first introductory chapter, this document contains four more chapters. Each chapter can gather one or more goals of this thesis.

The second chapter briefly describes the theory referring to the world of microwave filters based in cavities and waveguides, where different quantities of importance are described and the current major challenges concerning the design on tunable filters are presented. An example of a basic coaxial tunable filter is given at the end of the chapter.
The main objective of chapter 2 is to present the basics on 3D tunable filters and, additionally, to have a general knowledge about microwaves filtering. In this chapter, the theory itself is the goal.

The third chapter is dedicated to the design of the tunable filter of single tuning element under study. All the aspects related to tunable filters are evaluated through simulations. An electromagnetic software simulator is used in order to design, create and simulate the filter. This software is the *High-Frequency*

Structure Simulator (HFFS) from *Ansys*.
The objectives concerning chapter 3 are related to the understanding and acquisition of the methodologies when designing a 3D RF component, such as the one concerning this project, using inverse engineering. Moreover, this will let us understand and see how the theory is applicable in this type of structures.

The fourth chapter covers the measurements of a fabricated prototype of the filter with a network analyzer. The actual S-parameters and response of a real implementation of the filter are shown.
This chapter tries to show how the filter is finally assembled and adjusted. Also, a goal of this chapter is to compare the simulated response with the actual filter response.

Finally, last chapter is dedicated to the conclusions of the work. Also, possible future work on this project is explained.

Chapter 2

Fundamentals on 3D tunable filters

This chapter presents the basic concepts behind RF 3D filters. A brief introduction in RF microwaves filters is done at the beggining to lately introduce the main capabilities and applications of this kind of electromagnetic components.

Major challenges in the design of tunable filters are presented and an example of a coaxial tunable filter is shown and explained at the end of the chapter.

2.1 Technologies and applications of RF components

It is well-known, in microwaves world, that almost all off-chip devices are implementable in different technologies. These technologies are, basically, 3D components (waveguides, cavities, ...), distributed components (microstrip, CPW, ...) or distributed-piezoelectric components (SAW, crystals, ...). Nowadays, the decision of which technology should be used for a new component lies directly on the application. In table 2.1 there is a summary of the different advantages and disadvantages of each technology.

General RF technologies		
3D Components	Distributed Components	Piezoelectric-based Components
Very High Q_0 (>5000)	Low Q_0 (≈150)	High Q_0 (≈1000)
Very Low Losses	Moderated Losses	Low Losses
Large Volume	Large Size	Small Size
High Cost	Low Cost	Low Cost

Table 2.1: General comparison of RF technologies

Each technology has its own strengths and weaknesses, totally different from the others. For this reason, the selection of the technology is related with the requirements of the applications. For example,

in mobile communications that the whole transceiver is required to be very small, the best option could be using acoustic wave technologies such as SAW. In the other hand, in satellite applications where the requirement is to have minimum losses and volume can be sacrificed, the best option is to use 3D RF components such as waveguides or cavities. Planar technologies are typically used in prototyping and electronics based on Printed Circuit Boards (PCBs).

2.2 General definitions in Microwave Filters

Before getting into detail in the theory of 3D filters, it is interesting to know the basic concepts behind the world of microwaves filters.
The largest part of filters can be described as M-port networks with a number of N resonators. The response of a filter at the point of what we could define as "output port" is, somehow, a selection of the most interesting part of its inputs. In the major part of the cases, we are talking about electromagnetic waves.

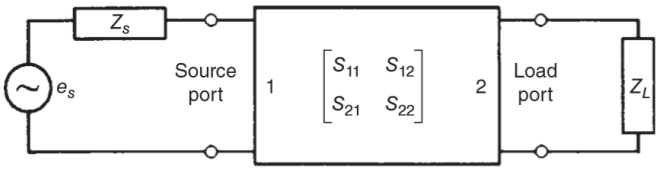

Figure 2.1: A basic two port network

These resonators and their external coupling with source and load at the ports will construct the band of interest, even a passband or a stopband. This kind of responses are crucial in many applications, avoiding interference and spurious in a system [4].

Filters can be built following different topologies. With topology, we are referring on how the resonators are allocated within the physical filter and how they are coupled between themselves. Different topologies can have the same response, so different ways to allocate the resonators could be possible. However, the resonant structures or the couplings might be necessarily different.

An example of coaxial filter is shown in figure 2.3. We can find 4 resonant elements and 5 coupling elements, where 3 of them are apertures and 2 of them are the input and output couplings at the ports of the filter.

A possible response of this topology is found in figure 2.4. This is a general Chebyshev response with 4 resonators that are translated into 4 reflection zeros. This type of response is characterized for having a good response in the stopband, but with a ripple in the bandpass. Other kind of responses such as the Butterworth or the Elliptic are examples within others.

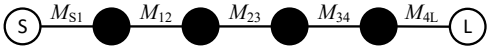

(a) In-line topology of 4 resonators

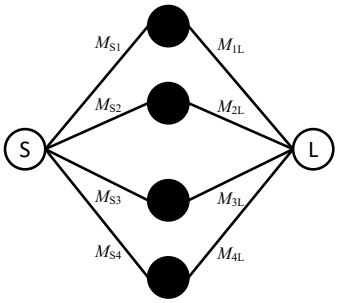

(b) Transversal topology of 4 resonators

Figure 2.2: Two examples of topologies. Black balls: Resonators. Black lines: Couplings.

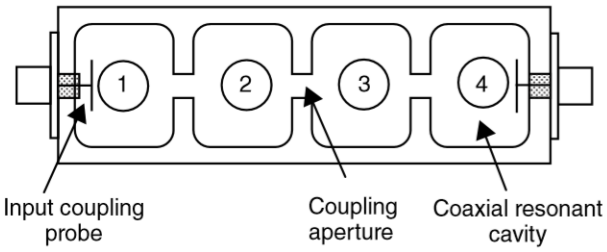

Figure 2.3: Example of In-line Coaxial filter with 4 resonators [1]

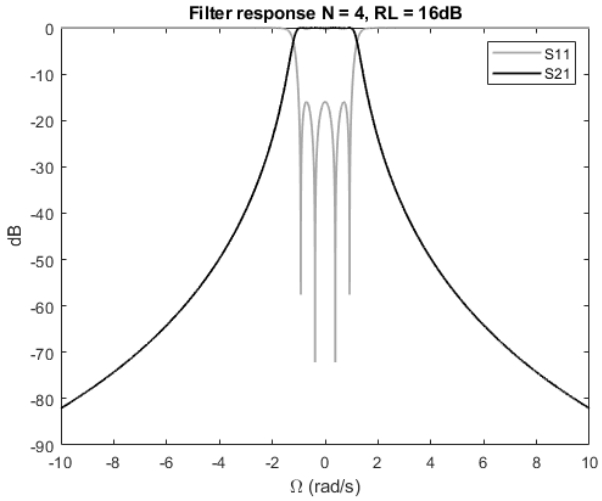

Figure 2.4: Chebyshev filter response of the equivalent lowpass prototype with 4 resonators

2.2.1 General steps in the synthesis and design of a filter

In order to comprehend better and complement the other sections of this thesis, a general overview on how the synthesis and design of a filter is done. A general step-by-step is shown in figure 2.5.

We will not go deeper in the procedures inside this step-by-step. However, the interesting part of

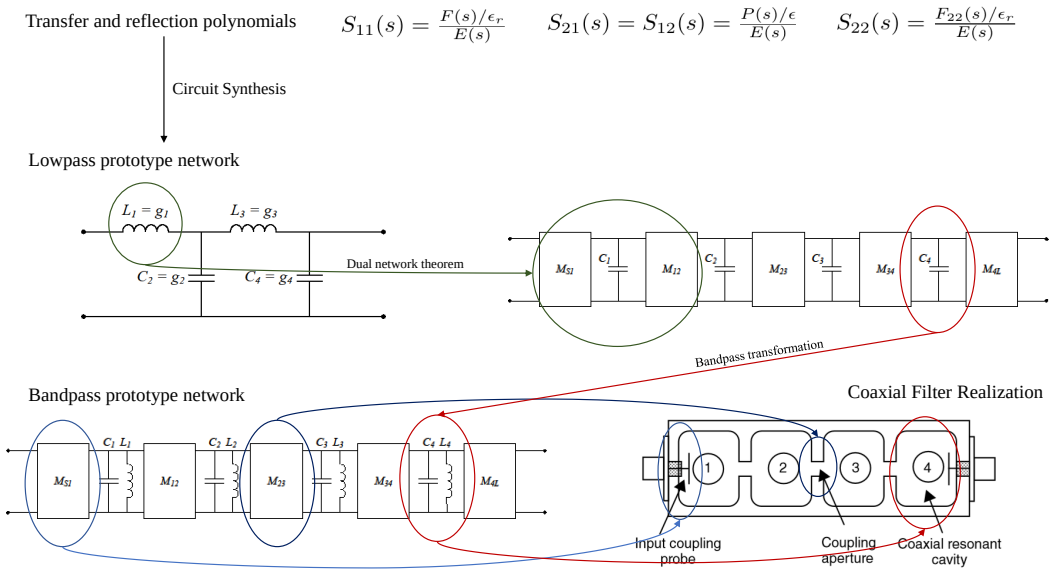

Figure 2.5: Steps of the synthesis process for a fourth-degree coaxial resonator bandpass filter

this general figure is that each one of the elements of a filter is individually designed following what the synthesis requires. Starting from the desired S-parameters, the circuit synthesis of the lowpass prototype is carried out and the necessary normalized couplings M_{ij} between elements i and j are obtained. After some transformations to the equivalent bandpass model, the extraction of the parameters needed is done. Finally, and depending on the type of technology used, the filter can be realized and manufactured.

2.2.2 Unloaded Quality Factor

Physical losses in a non-radiating RF component can be addressed to, what we call, quality factor (Q). This quantity relates the capability of a resonant structure to store the energy and the energy dissipation that occurs in it in a period of time. A general definition could be found in equation 2.1.

$$Q_0 = \omega_0 \left(\frac{\text{energy stored}}{\text{average power loss}} \right) = 2\pi \left(\frac{\text{energy stored}}{\text{energy dissipated per cycle}} \right) \tag{2.1}$$

where Q_0 is the unloaded quality factor at the frequency of resonance ω_0.

However, this prescription of the Q_0 is traditionally encumbered with difficulties in identifying the stored energy of a general electromagnetic structure. An accurate calculation would require knowledge of the conductivity of the metal walls as well as the dielectric loss tangent within other physical characteristics of the implemented filter. Typically, high-conductivity metals such as gold and copper are used to achieve high Q values. There are many ways to extract the value of the unloaded Q by means of the measured S-parameters, as demonstrated in [1].

2.2.3 Couplings

Electromagnetic couplings between elements are important quantities to control when designing a filter. The amount of electromagnetic field that one element couples to another element has several effects in the frequency response. These coupling can be from resonator to resonator (interresonator couplings), from input/output port to resonator or even between input and output ports. For this reason, the design of a filter can be performed mainly in two ways, thanks to the two main elements of a filter (resonators and couplings). In one hand, designing the resonators in such a way that each one of them constitutes one of the desired poles of the band, therefore each resonator has its own resonance frequency. This is done while maintaining a unitary coupling coefficient M_{ij}.
In the other hand, what we call synchronous coupling resonators, that basically consists in the usage of equal resonators, which resonates at the same frequency, and the distribution of the band, in this case, is done by means of the coupling coefficient M_{ij} that is not unitary as in the previous case.
Even a combination of both approaches is possible to implement, but complexity grows.

2.2.3.1 Interresonator Coupling

Physically, the coupling between two resonators will do that the resonances separate in frequency, occurring what we call *split*. The coupling coefficient, then, is somehow a measurement of the separation in frequency of both resonances. In a general case, the physical coupling coefficient between element i and j can be calculated with the expression in equation 2.2.

$$K_{ij} = \frac{f_e^2 - f_m^2}{f_e^2 + f_m^2} \tag{2.2}$$

where f_e and f_m are the resonance frequencies computed from the evaluation of the even and odd mode circuits. For a two pair of coupled resonators, the theoretical obtainment of these frequencies depends on the nature of the coupling, if it is inductive or capacitive. In reference [1], both approaches are demonstrated. These two frequencies are the resulting ones of the split. In general, $f_e > f_m$ for inductive coupling and $f_m > f_e$ for capacitive coupling. Actually, only the magnitude of the coupling is needed.

This value of physical coupling can be normalized to the fractional bandwidth in order to obtain the coupling element M_{ij} that is typically used in synthesis procedures [1].

$$M_{ij} = \frac{f_0}{BW}\frac{f_e^2 - f_m^2}{f_e^2 + f_m^2} \tag{2.3}$$

where f_0 is the central frequency of the band. Notice that this central frequency f_0 - considering a filter based in equal resonators - is the resonance frequency f_r of an individual resonator.

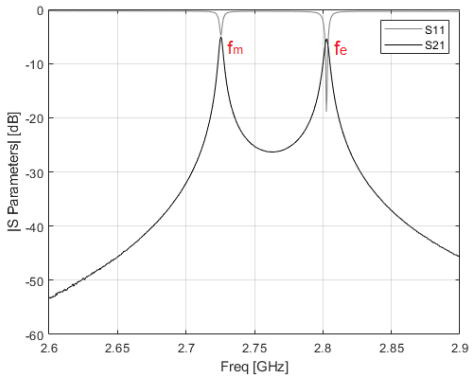

Figure 2.6: Example of a split of resonances

2.2.3.2 External coupling

The external coupling refers to the way the input and output ports load the circuit. This coupling, that must be considered in the synthesis procedures, has a big impact in the final response of the filter. This loading effect has an impact in bandwidth, group delay and quality factor. Actually, these three quantities are related as we will see in this chapter and demonstrate throughout this thesis.

This effect can be quantified with the external Q, Q_{ext}. There are several methods to determine this external Q-factor, but we will focus in the group delay method. The group delay τ is calculated as the derivative of the phase with respect to frequency, which can be also related with Q_e as equation 2.4.

$$\tau = \frac{\delta\phi}{\delta\omega} = \frac{4Q_e}{\omega_0}\frac{1}{1+(2Qe(\omega-\omega_0)/\omega_0)^2} \tag{2.4}$$

If the group delay is evaluated at the resonance frequency ω_0, the resulting expression gets simpler. As seen in equation 2.4, the maximum group delay is given at the resonance frequency. So, the external Q_e can be obtained with expression 2.5

$$Q_e|_{\omega_0} = \frac{\tau\cdot\omega_0}{4} \tag{2.5}$$

Parallel to this, considering a filter where the Input/Output ports only load a single resonator, bandwidth could be obtained using the equation in 2.6

$$Q_{e_{in}} = \frac{g_0 g_1}{FBW} \tag{2.6}$$

where g_i are the lowpass prototype immitances defined in the circuital synthesis of the filter. Concretely, the immitances defining the input coupling M_{01} from element 0 (source) and 1 (same applies for the output port). Therefore, the expression can also be expressed as 2.7.

$$Q_{e_{out}} = \frac{g_n g_{n+1}}{FBW} \tag{2.7}$$

Those immitances values can be used to compute the necessary normalized coupling value as expressed in equation 2.8.

$$M_{ij} = \frac{1}{\sqrt{g_i g_j}} \tag{2.8}$$

2.2.3.3 The coupling matrix

The actual realization of a filter can be performed by different approaches. By using the Coupling Matrix approach, firstly introduced by Atia and Williams in the 1970s and explained in detail in [1], a bandpass filter can be fabricated. The basic idea behind this matrix is to characterize all relations between elements of the filter in a matrix form. This approach quantifies each of the couplings needed between elements of a filter to obtain a desired response in frequency. The normalized coupling M_{ij} quantify the necessary coupling between elements i and j of the filter. Then, M_{ij} can be related to the physical coupling K_{ij} with equation 2.3. A N-degree bandpass filter would require a matrix of $(N+2) \times (N+2)$ dimension if the input and output couplings from source and load are considered.

$$\mathbf{M} = \begin{pmatrix} M_{SS} & M_{S1} & M_{S2} & M_{S3} & M_{S4} & M_{SL} \\ M_{1S} & M_{11} & M_{12} & M_{13} & M_{14} & M_{1L} \\ M_{2S} & M_{21} & M_{22} & M_{23} & M_{24} & M_{2L} \\ M_{3S} & M_{31} & M_{32} & M_{33} & M_{34} & M_{3L} \\ M_{4S} & M_{41} & M_{42} & M_{43} & M_{44} & M_{4L} \\ M_{LS} & M_{L1} & M_{L2} & M_{L3} & M_{L4} & M_{LL} \end{pmatrix} \tag{2.9}$$

Figure 2.7: An example of $N+2$ coupling matrix, considering a 4 degree filter

The key fact of having a matrix approach is that several matrix operations can be realized. Therefore, different configurations of the matrix can lead to the same response of the network. Several methods are explained in the literature [1] to reconfigure this matrix and obtain different filter topologies. However, not all the configurations are feasible to implement in real world.
Notice that, in the elements of this matrix, the quantities of K_{ij} and Q_e are implicit.

2.3 Tunable Filters

2.3.1 Major challenges in the design of 3D tunable filters

Over the past two decades, several publications have been reported on tunable filters [[5]-[6]]. The majority of them are based on microstrip technology. The disadvantatge regarding microstrip filters is that they do not accomplish the stringent requirements of high-Q applications, moreover the achievable Q degrades further once the filter is integrated with tuning elements. Concerning three-dimensional filters, such as the one this thesis is about, several publications demonstrate the possibility to use tunable 3D filters.

In general, the main challenge concerning tunable filters involve maintaining features over the whole tuning range. Specifically, in the case of 3D tunable filters, the matter goes around bandwidth and losses [7].

Maintaining a constant bandwidth over the tuning range might be not as easy as we would like. The tuning mechanism should be synchronized with the set of couplings in order to maintain a constant bandwidth. In one hand, if the external coupling is modified by the coupling mechanism over the tuning range, the bandwidth will not be constant as the group delay would not be the desired one in all frequencies. In the other hand, if the interresonator couplings are modified by the tuning mechanism, the split effect on the resonators would change the bandwidth. Tuning elements could be added to the design at the coupling mechanisms, in order to control and maintain the constant value of the couplings while the resonance frequency is also tuned. However, this solution might not be the best due to the fact that adding tuning elements could be translated into Q degradation and grow in size. For this reason, designing tunable filters with absolute constant bandwidth and without Q degradation is a major challenge in three-dimensional filters.

In another plane, the size and the power handling capabilities might be requirements that should be taken into account. Size is a very constraining factor in the world of RF and the power that a component can handle is very related to this.

2.3.2 Principles of tuning in a Coaxial Filter

2.3.2.1 Coaxial Filters

In this section, we will discuss the main parameters concerning the design of a coaxial filter. A coaxial filter is a filter based in cavities or waveguides. In each of its cavities a coaxial resonator is placed and by means of different coupling techniques, the filter is constructed.

Several publications concerning the design of coaxial filters are found in the literature. An example of a coaxial resonator designed for the S-band can be found in [8].

Figure 2.8: Commercial Filter example from Lorch Microwave

Different examples of coaxial filters can be found in this thesis in figures 2.3 and 2.8. The last one is a little bit more complex, but it is a good example to see different coupling techniques and a new topology that we have not presented yet. Without entering in too much detail, this last filter from Lorch Microwave is a coaxial filter with 8 resonators that uses a topology of cascaded quadruplets. In general, the main line is coupled resonator to resonator, using windows in each of its cavities. These windows are perturbed by means of screws placed at the roof of the filter, perfectly controlled in order to adjust the coupling coefficients.

Another interesting thing about this particular case is that there are some resonators, that in an in-line topology would never *see* each other, but in this particular case they do. We are talking about the resonators that we could label as 1 and 4 and 5 and 8, seen from the input port. They are coupled using a capacitive technique or, in the same sense, an electrical coupling. When designing the RF component, these cross-couplings are extracted from the synthesis procedures such as the Coupling Matrix approach.

2.3.2.2 Coaxial Resonator

A coaxial resonator - also known as combline resonator - is a resonant structure that consists in a metallic post placed at the center of the cavity.

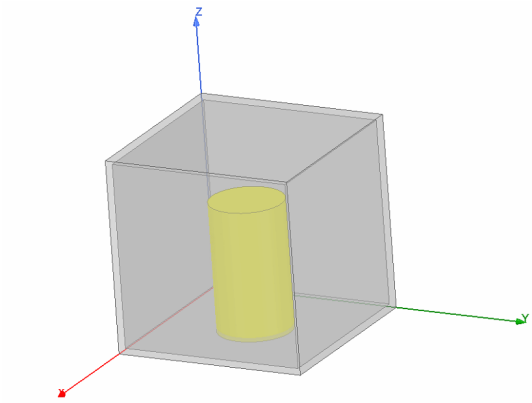

Figure 2.9: One single 3D cavity. In it, a coaxial resonator post of $\lambda/4$

This resonator is short-circuited with the bottom ground of the cavity and its length is defined to be

$\lambda/4$ at the desired resonant frequency or shorter. From the grounded roof of the filter, the resonator is not connected, so a capacitive effect appears. This capacitive effect can be modeled as a capacitance C_a as shown in figure 2.10.

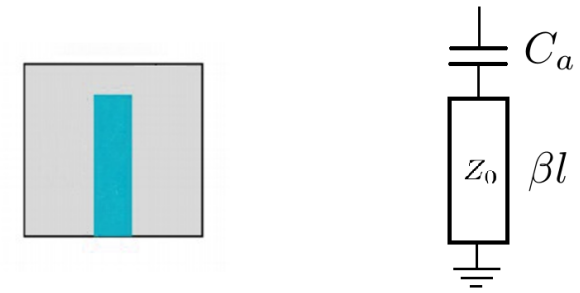

Figure 2.10: Cross section of the coaxial resonator and its equivalent circuit

At resonance frequency, the total admittance of the transmission line with the capacity must be zero. Hence,

$$\frac{Y_0}{j\ tan(\theta_0)} + j\omega_0 C_a = 0 \tag{2.10}$$

Isolating C_a from expression 2.10, for an electrical length at the resonance frequency of $\beta l|_{\omega_0} = \theta_0 = \pi/2$, that is a $\lambda/4$ transmission line, C_a must be 0, enforcing the roof to be at infinite distance from the metallic post (no capacitive effect should be present). Therefore, C_a can control the resonance frequency of the resonator once it is present, being this the reason behind the fact that the post must be equal or shorter than $\lambda/4$. Thanks to that, once the filter is manufactured, it is quite easy to adjust the resonances and correct fabrication tolerances by means of metallic screws placed at the roof, over the metallic posts. These screws can tune the capacitive effect from the roof to the $\lambda/4$ resonator and once the filter is adjusted as desired, the screws are fixed.

2.3.2.3 Fields distribution and coupling techniques

It might be obvious that the resonant coaxial cavity will allow the excitation of several electromagnetic modes in it. The metallic post enforces the structure to allow only the propagation of certain modes accomplishing some boundary conditions. As the metallic post is directly short-circuited to the external metallic ground, currents are forced to be maximum there while currents are forced to be zero at the opened end. Considering this, the E-field will be maximum at the opened end of the metallic post while the magnetic field will be maximum at the connected end of the metallic post, being this the boundary condition that allows the excitation of the fundamental mode of this structure. Notice that the fundamental mode is a TM mode, as the electric field is oriented along the direction of propagation.

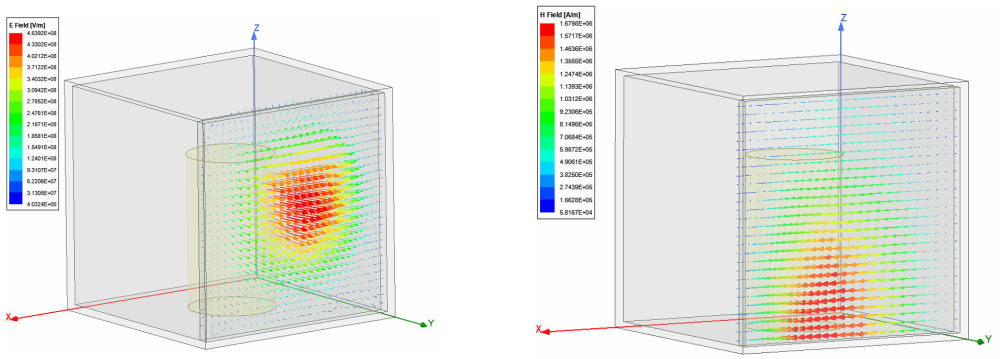

(a) Electric Field (b) Magnetic Field

Figure 2.11: Fields distribution of the fundamental mode

Considering this fundamental mode as the one concerning our design, the coupling used will depend on the desired response and the synthesized coupling matrix. A typical coupling technique for cavity filters is, basically, a coupling window. This coupling window modules the amount of field that one resonator *delivers* to the other.

If the interest is around a coupling mainly electric, the window used must be centered where the maximum of electric field is found. If the interest is around a magnetic coupling, the coupling window or technique must be centered where the maximum magnetic field is found. Different examples of coupling windows are found in figure 2.12.

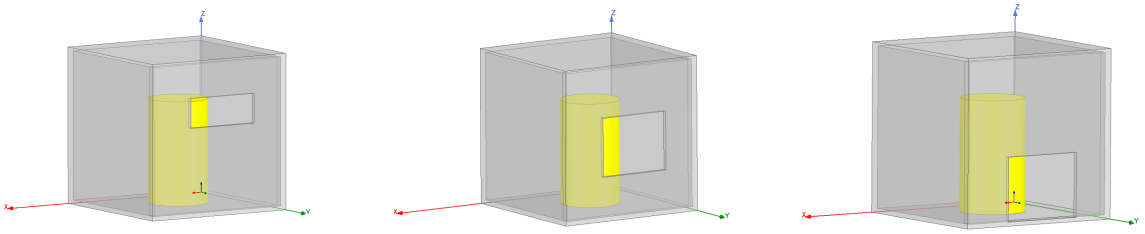

(a) An electric window coupling (b) An hybrid window coupling (c) A magnetic window coupling

Figure 2.12: Three examples of coupling windows

The dimensions of the coupling window depend on the value of physical coupling K_{ij} desired to implement.

Another example of coupling technique is found in 2.13. This coupling technique consists in a physical window with a perturbation in it. This perturbation is a screw that can be tuned in order to have a fine adjustment of the physical coupling once it is fabricated. In this particular case, the screw is used to modify the electric coupling between resonators.

This last coupling technique is used in the Lorch Microwave 8 pole filter from figure 2.8.

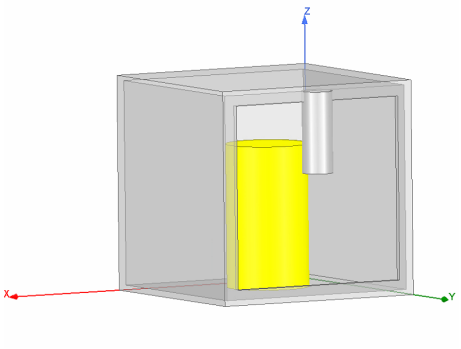

Figure 2.13: Example of a coupling technique: Coupling screw

2.3.2.4 Tunability in Coaxial Filters

In order to create a resonant cavity with tuning capabilities, several options appear. Depending on the desired tunable parameter, the techniques used in the design might be different. The most typical parameters to tune are central frequency and bandwidth. Since the capability of interest regarding this thesis is the frequency tuning, this will be the topic to be discussed in this section.—— The most intuitive and easy technique in terms of design is to use the same principle that we explained before. By means of metallic screws or tuning disks over the resonators, we are capable to change the effective capacitance over it and, therefore, modify the resonance frequency of each individual resonator.

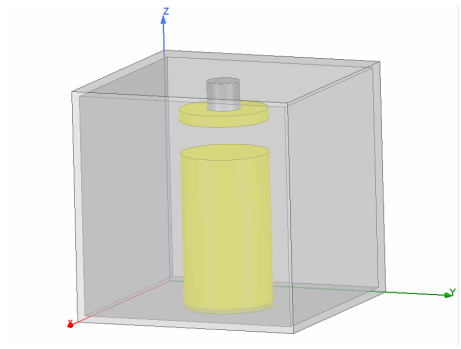

Figure 2.14: 3D model of a combline resonator with a tuning disk

This provides a considerable wide tuning range without growing too much in complexity. However, the use of this kind of tuning techniques might lead to Q-degradation and, therefore, an increase of losses. The tuning mechanism requires to have a discontinuity in the structure that is reflected in the effective Q-value. Moreover, while the gap is decreased, the capacitive effect gets more importance and more electric field is discharged at the tuning disk, adding more losses to the system.

Therefore, it is obvious that a N-order coaxial filter would require a number of N tuning disks. Each resonator would require its own tuning mechanism and they would need to be tuned together and synchronously. In general, this would lead to a grow in complexity and losses.

Chapter 3

Design of a High-Q tunable filter with single tuning element

Several designs of three-dimensional tunable filters with High-Q and constant bandwidth have been implemented. Different techniques can be found, using MEMS or piezomotors [9]-[10] to control the tunable elements. However, the realization of these filters has a big counterpart, they depend on many tunable elements. These elements need to be tuned in a synchronous way. If not, the desired response might be distorted.

This chapter covers the 3D design of a High-Q tunable filter with a single tuning element. At first, an introduction to the [[2]- [11]]'s filter idea is done. Then, an analysis of the elements of the filter is carried out by means of the quantities presented in chapter 2. While doing this, an study in order to understand the reasons behind the shape and form of each of the elements is realized. At the end of chapter 3, the final response of the filter in HFSS is presented over the tuning range.

3.1 High-Q Tunable Filter with single tuning element

The design of High-Q tunable filters is a demonstrated reality as several designs can deal with this requirement by far [12]. However, some aspects that might be necessary to work on are the required number of tuning elements and the mechanism itself. In almost all designs a number of tuning elements at least equal to the number of resonators is needed. The example explained in previous chapter is the clear example of that. A combline filter, as demonstrated in [10], is capable of holding a high quality factor over the entire tuning range, however the minimum number of tuning disks needed is equal to the number of resonators. For an N-order filter (N resonators), N tuning elements as minimum.
As we stated in previous chapter, adding tuning elements can increase losses and complexity. More tuning elements means more complexity in adjusting the filter at the desired central band. We have to take into

account that each tuning element is individual and if we want to sweep the N reflection zeros of the band together, they should be moved synchronously. When designing a 2-order filter, the problem on the tuning elements might not be so important, but the problem grows exponentially when designing a RF multiplexer, hundreds of resonators to handle.

The proposed idea of [2] tries to readapt the concept of the combline tunable filter. The general idea is the same, modify the capacitance seen from the metallic post to the grounded walls. However, the tuning mechanism is totally different. By giving an elliptical shape to the cavities and treating the resonator post as a floating element, tunability is achieved.

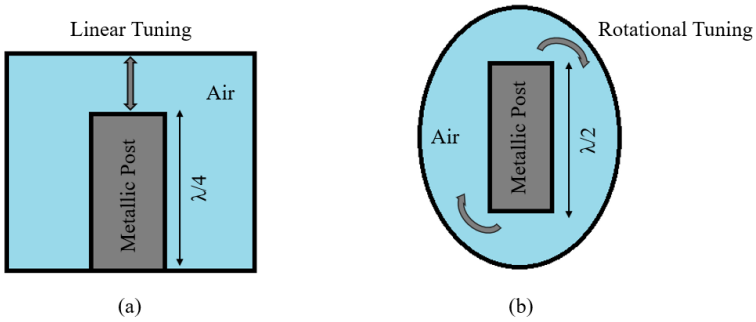

Figure 3.1: Cross section of a coaxial resonator a) Conventional quarter wavelength resonator with linear tuning, b) Proposed half-wavelength resonator with rotational tuning

For proof of concept, in [2] and [11] a 4-pole filter is designed considering a central frequency of 2.5 GHz with a fractional bandwidth of 4%. The proposed filter is designed to have a tuning range of 30% with an insertion loss (IL) variation of less than 0.02 dB over the entire tuning range.

In order to achieve a rotational tuning, the metallic posts are hold by means of a dielectric rod that acts as the unique tunable mechanism. A 3D design made in HFSS can be found in figure 3.2.

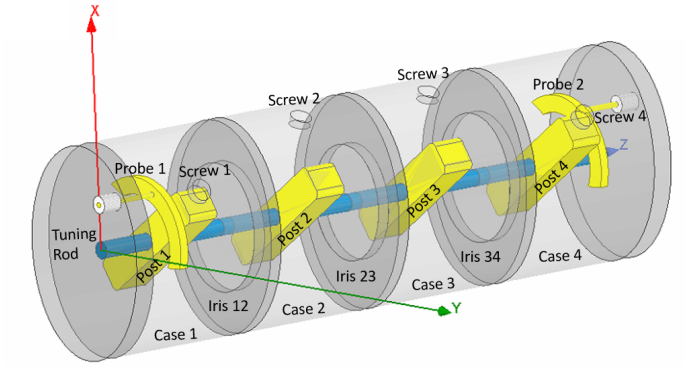

Figure 3.2: 3D model of the proposed tunable coaxial filter in [2]

Elliptic parts	**Major Axis**	**Axes Ratio**	**Thickness**
4 Cavities	50	0.75	35
Iris 12 (= Iris 34)	30	0.85	3
Iris 23	27	0.85	3
Metallic post	**Length**	**Width**	**Thickness**
Post 1 (= Post 4)	35	8	8
Post 2 (= Post 3)	34.76	8	8
Tuning mechanism	**Diameter**		
Rod	4		
Input/Output Probe	**Angle**	**Gap**	**Thickness**
2 Shaped Probes	114	0.5	2.1
Fixed Screws	**Location**	**Depth**	**Diameter**
Screw 1 (= Screw 4)	50	2.7	5
Screw 2 (= Screw 3)	15	2.4	5

Table 3.1: Dimensions of the proposed tunable filter in [2] (dimensions in "mm", angles in "deg")

3.2 Analysis of the design of the proposed filter

3.2.1 Definitions of the analysis under study

In order to streamline the analysis process, certain elements of the analysis need to be defined.

3.2.1.1 HFSS solution types and simulation setups

Firstly, the different **solution types** that HFSS software provides. Depending on the EM problem wanted to solve, one solution type might be more accurate than others. In this chapter, two solution types are used:

- **EigenModes**: This solution type is used for calculation of the eigenmode of the structure and its resonant frequency. It analyzes the resonant structure itself, so no ports are needed. Additionally, the fields of the corresponding resonance frequencies can be plotted on/in the structure.

- **Driven Modal**: This solution type is used for calculation of the S-parameters, based on modal analysis, for a passive high frequency structure which is driven by a "source". In this solution type, the definition of the ports is necessary.

Both solution types require a simulation setup according user's preferences. The simulation setup basically determines the precision and time of simulations. A more accurate solution requires more simulation time. Quantities such as mesh size, frequency range, number of points and other general simulation settings are defined. In general, a balanced simulation setup in terms of time and accuracy is used with a maximum mesh size defined by the wavelength of the highest simulation frequency. For specific simulations that require high accuracy, a more precise simulation setup is defined.

3.2.1.2 Coupling matrix

The purpose of this chapter is to design a similar replica of the proposed filter in [2] and analyze its performance. Therefore, the prototype 4-order filter desired to implement in this thesis will also fall in the band of 2.5GHz with an absolute bandwidth of 100MHz and return loss of 16dB. An in-line topology will be considered and the filtering function desired to implement will be an all pole Chebyshev's filter response. For these reasons, a coupling matrix is synthesized by using a direct synthesis of the coupling matrix method defined in [1]. The coupling matrix can be found in appendix A.1. This synthesized matrix will help in the analysis and the design, as it will give several hints of the reasons behind the shapes and dimensions of the proposed filter in [2].

3.2.1.3 Variable quantities for design purposes

An important parameter that needs to be defined is the rotation angle α that we will work with. This angle will define the direction of the metallic posts in the structure in the plane XY of our models. Its origin ($\alpha = 0$) is defined to be in the x-axis as follows:

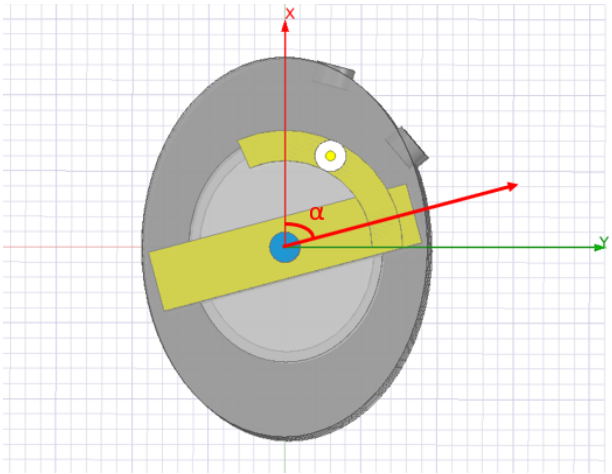

Figure 3.3: Alpha definition

Notice that all resonator posts will be totally aligned, so one rotation angle is enough.

3.2.2 Resonant structure

The basic resonant structure is the cavity with the metallic post inside. This cavity is made of a conductive material that we defined to be aluminum. In it, a dielectric material (air) fills the cavity. Notice that, the cavity could be seen as an elliptical waveguide with a perturbation (metallic post) in it.

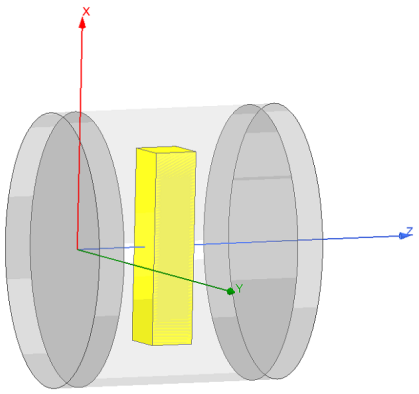

Figure 3.4: 3D model of the resonant cavity in HFSS

The metallic post is defined to be a cylinder of length equal to $\lambda_g/2$. As we are in a guided medium, we are talking about guided wavelength λ_g. Since the post is not lying on the grounded floor of the cavity, some boundary conditions must be accomplished that justify this length, as we will see throughout this section.

Notice that the structure is an elliptical cross-section waveguide, allowing the excitation of modes along the major axis and the minor axis, depending on the eccentricity of the ellipse. Considering Mathieu functions of first kind and the definition of elliptical waveguide modes given in [13] and [14], modes in elliptical waveguides are defined as TM_{cmn}, TM_{smn}, TE_{cmn} and TE_{smn}, where the first subscript c or s denote the mode as cos-type or sin-type respectively, depending if the longitudinal field is symmetric along the major axis or minor axis. The second subscript represent the order of Mathieu function of first kind and, finally, the last subscript defines the n_{th} parametric root of the function.

Using the eigenmodes solution type of HFSS, this resonant structure at $\alpha = 0$ allows the propagation of modes of table 3.2 above 1GHz. These modes are the first four modes that the structure can excite. Notice that labeling these modes as cosine-type or sine-type might lead to confusion, as we will be dealing with a non-static waveguide (the metallic post will rotate, modifying the subscription of sine-type and cos-type).

In appendix A the fields distribution of each of the modes of table 3.2 are found. Notice that only the first mode defined (the first TE Mode) given by HFSS is interesting to us, as this mode is the only one that behaves as desired around the frequency of interest (2.5GHz). The maximums of electric field are in the ends of the metallic post, giving chance to the rotational tuning mechanism to work. Conjugately

Allowed modes within 1GHz and 6GHz		
Eigenmode	Frequency [GHz]	Q_u
Mode 1	2.911	6156.15
Mode 2	4.968	9404.81
Mode 3	5.037	9024.84
Mode 4	5.893	8574.11

Table 3.2: Allowed first four modes with its Q_u ($\alpha = 0$)

to this, magnetic field is maximum at the center of the cavity.

This mode might not be the fundamental mode that in an empty elliptical waveguide would exist. Notice that by adding the metallic post, it enforces the structure to allow only the existence of modes accomplishing some boundary conditions at certain frequencies. For the first mode found, the metallic post is enforcing the structure to be as figure 3.5.

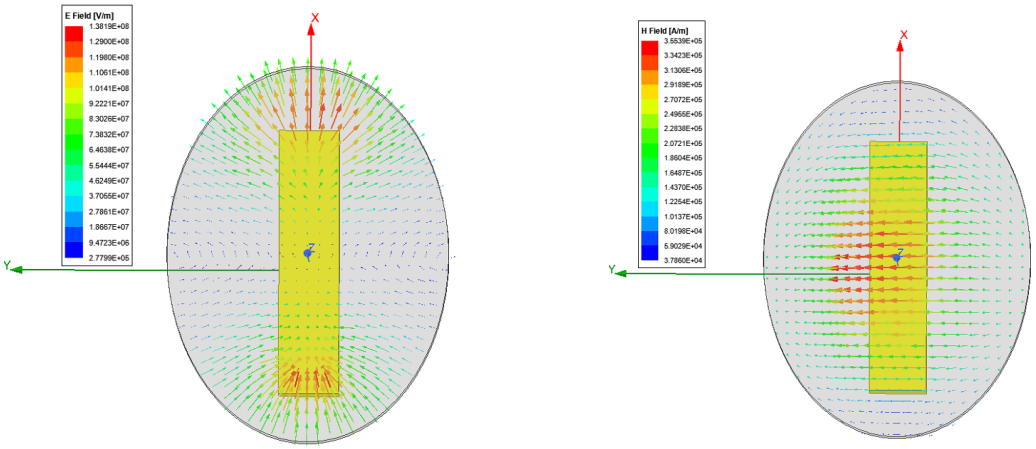

(a) Electric field distribution

(b) Magnetic field distribution

Figure 3.5: Fields distribution at $\alpha = 0$

Other parasitic capacitances at some frequencies might appear between the lateral walls of the metallic post and the grounded walls of the filter, allowing, then, the excitation of other modes accomplishing this other boundary condition as seen in appendix A.

A parametric sweep of the rotation angle α (from 0^o to 90^o) versus the first eigenmode is done, the resulting plot is in figure 3.6. The elliptic shape of the cavity defines the tuning capacitance that fixes the central resonance frequency. It is shown that, by means of decreasing the *gap* between post and external wall, the resulting capacitive effect is amplified and, for this reason, the resonance frequency decreases. The same happens with the quality factor. When the electric field intensifies, losses also increase.

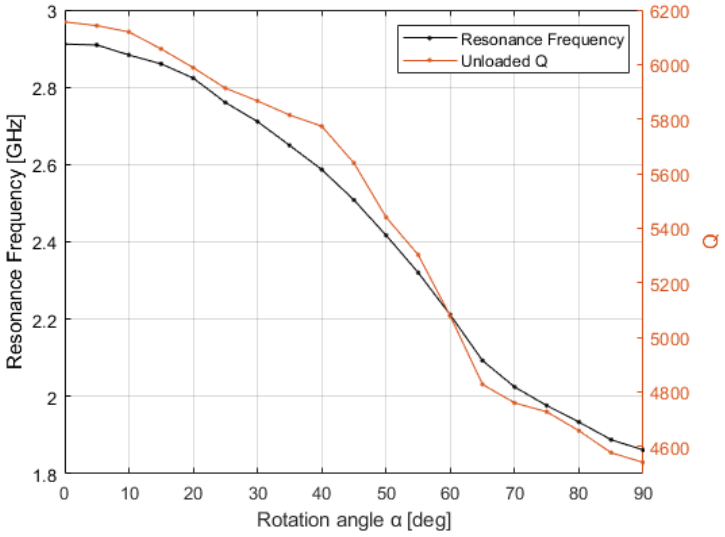

Figure 3.6: Resonance frequency and Q

However, the electric field distribution over the resonator is not uniform in all the rotation angles. If α is increased (or decreased), the electric field distribution tends to focus to one of the edges of the resonator. This effect appears in figure 3.7.

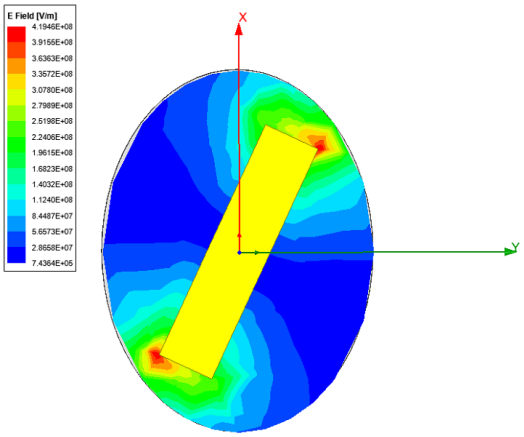

Figure 3.7: Electric field distribution at $\alpha = 25°$ - Magnitude

In order to have a cleaner sweep in frequency, these edges should be soften as figure 3.8.

With this correction, the electric field over the resonator is more uniform than before. It is obvious that complete uniformity is not possible to achieve, as one of the edges will be always closer to the external wall than the other at some rotational angles, but better results are obtained. Additionally to this, the resulting Q is slightly better than before and f_r shifted to higher frequencies.

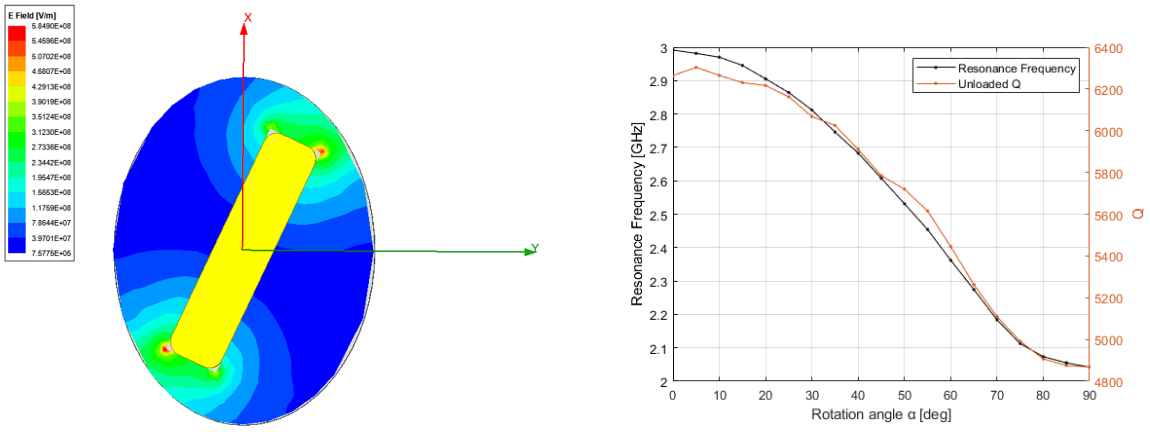

(a) Electric field distribution - Magnitude

(b) Resonance Frequency and Q

Figure 3.8: Effect of the cut in the edges

3.2.3 Interresonator Couplings

The study of the interresonator coupling is carried out by means of the EigenModes simulation type, as previous section. The coupling is mainly magnetic, so coupling irises as figure 3.9 are used.

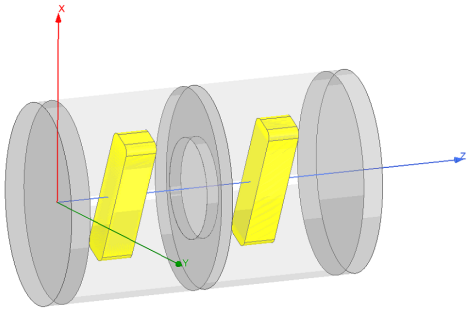

Figure 3.9: 3D model of two resonators coupled by a coupling iris

As studied in chapter 2, the coupling between two resonators produces a split effect in frequency. So that, the central frequency of resonance of both resonators (assuming that they are equal) is divided in two, the even and odd mode frequencies. These coupling irises are centered where the maximum of magnetic field is found. Therefore, the rotational tuning is achieved by means of the electric field while the distribution of the band (the split of frequencies) is done by means of the magnetic field.
Using the values of the first iris (Iris 12) given by the authors of [2], the sweep in frequency of both resonances is found in figure 3.10.

With the values of the even and odd mode frequencies, we could obtain the physical coupling coefficient by means of equation 2.2.

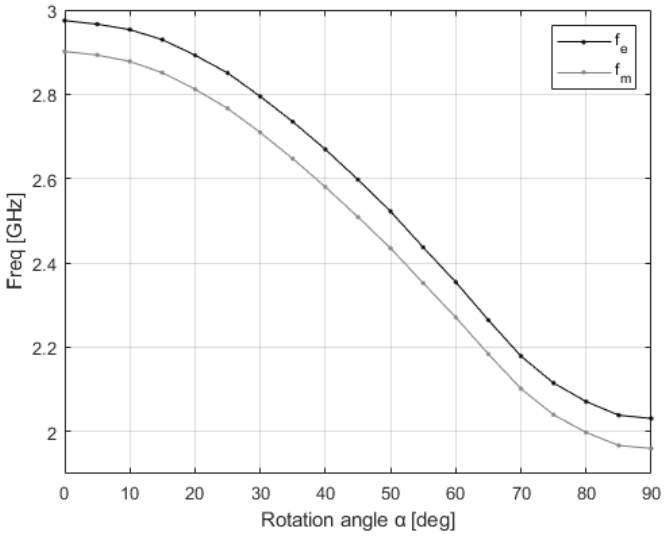

Figure 3.10: Eigenmode resonance frequencies for all α values

3.2.3.1 Designing the coupling iris

When designing the dimensions of the coupling iris, in order to avoid, as much as we can, modifying the filter response over the tuning range, an important value to consider is the product of $f_r \times K_{ij}$. If this product is constant over the tuning range, we could consider that the filter response in terms of distance between reflection zeros is constant. Notice from expression 2.3 that (assuming the same normalized coupling coefficient M_{ij} for all the bandpass responses in the tuning range) the product of $F_r \times K_{ij}$ should be constant to obtain a constant absolute bandwidth.
In this design, the elliptical shape of the cavity determines the resonance frequency of the resonators. To obtain a $f_r \times K_{ij}$ constant over the whole tuning range, seems intuitive to use elliptical irises. Thanks to this, we have two degrees of freedom in the design of the iris, the major axis and the axis ratio (minor axis / major axis).
In one hand, if the major axis is modified fixing the axis ratio —— therefore, the minor axis and the whole iris would be proportionally changed —— the coupling of the resonators would be modified as less/more field would be able to couple to the linked structure.
In the other hand, if the axis ratio is modified fixing the major axis —— therefore, the minor axis and the whole iris shape would be changed —— the coupling between resonators would be modified, but with different weight for each of the angles. The constancy of the product $f_r \times K_{ij}$, mostly, rest on this second point.

A good way to proceed here is, first, fixing the major axis value and looking for an axis ratio that gives approximately a constant value of $f_r \times K_{ij}$. Then, when this axis ratio is chosen, vary the major axis value to find the coupling value desired and given in the synthesis step.

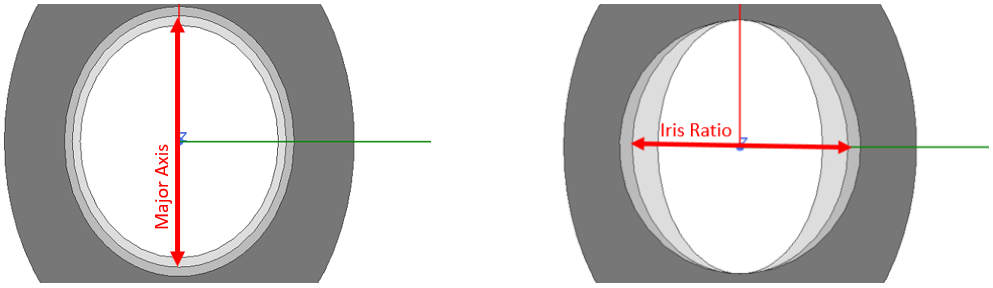

(a) Variation of the major axis (b) Variation of the iris ratio

Figure 3.11: Iris shape

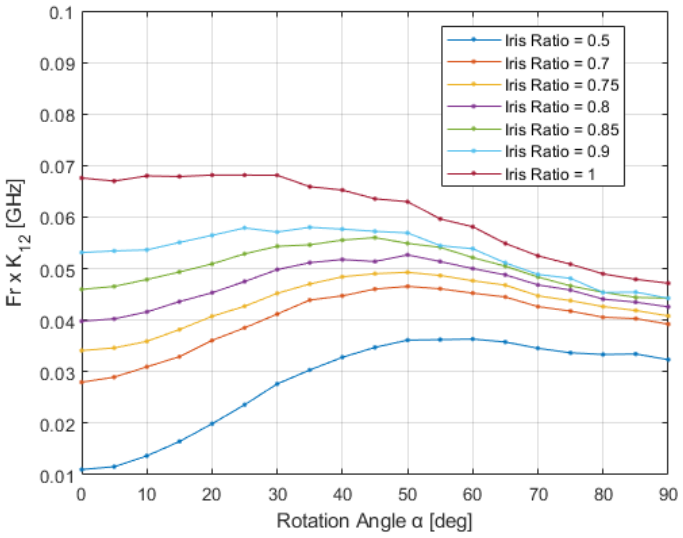

Figure 3.12: Interresonator coupling with different elliptic irises: axis ratio variation with fixed major axis to 25mm

From figure 3.12, we could extract that the axis ratios that better respects the constancy of the $F_r \times K_{ij}$ are the values of 0.8 and 0.85, the last one is the value that [2] chose.
We could state that by increasing the rotation angle, the product of $F_r \times K_{ij}$ tends to the same value for all the iris ratios. This is because we are using a coupling technique based in the magnetic field. For high values of α, the magnetic field lines cross the coupling iris mainly through the major axis, that is constant for all values of axis ratios used.

The results of the two coupling irises used in the entire assembled filter are shown in figure 3.14. Applying expression 2.3 and considering the required coupling coefficients given in A.1, the target values of the product $f_r \times K_{ij}$ considering an absolute bandwidth of 100MHz are $f_r \times K_{12} = 82MHz$ and $f_r \times K_{23} = 65.3MHz$. Notice from the synthesized coupling matrix of A.1 that K_{34} is required to be the same than K_{12} and f_0 in expression 2.3 is the resonance frequency of a single resonator f_r (the 4 of them are equal).

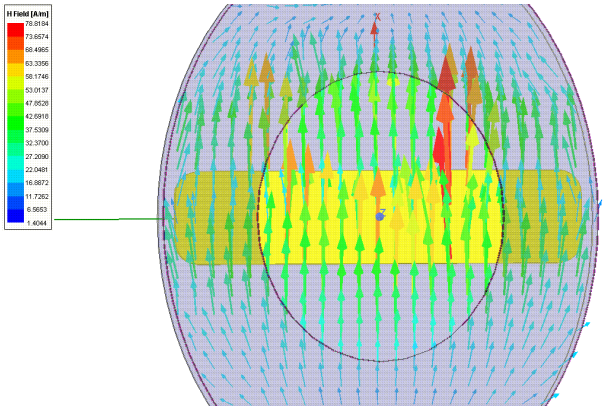

Figure 3.13: Magnetic field distribution for $\alpha = 90^{o}$

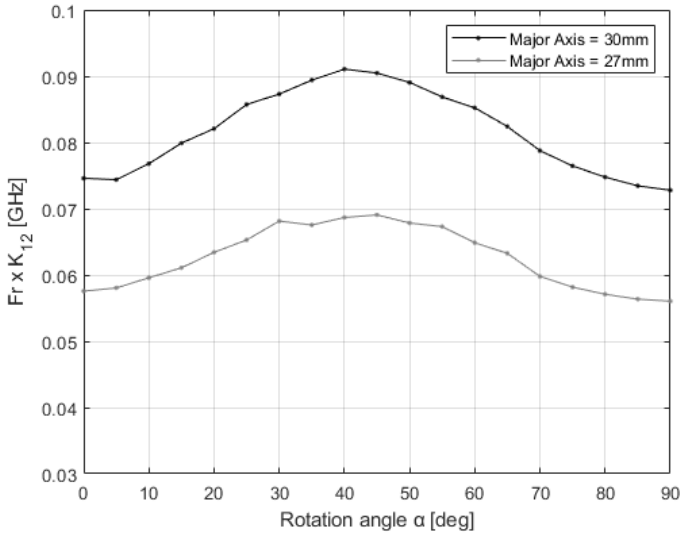

Figure 3.14: Interresonator coupling with different elliptic irises: major axis variation with fixed axis ratio to 0.85

A more or less constant value of the product $F_r \times K_{ij}$ is achieved for both irises, starting and ending in a similar point. The variation of the major axis controls the mean value of the coupling, while the axis ratio controls the shape of the coupling along the rotational angle.
Notice that the distance between resonators could be modified in order to have a different coupling coefficient. However, we would modify, then, the resonant structure designed at the previous step, invalidating the results obtained..

3.2.4 Tuning mechanism

One of the major challenges in this project is the tuning mechanism. It should provide a good rotational tuning without having a big impact in the electromagnetic properties of the structure.

Our purpose is to design a filter with single tuning element, this means that the resonators must be tuned together. The most intuitive way to accomplish these conditions is to tune the angle of the metallic posts by means of a central rod that crosses each of the posts and controls their angle. By introducing this rod, the resonant structure might be changed. The best option here is to introduce a dielectric rod with low relative permittivity ϵ_r and tangent loss $tan\delta$, but rigid enough to hold the metallic posts without losing its shape. For the HFSS study, a rigid PVC with $\epsilon_r = 2.7$ and $tan\delta = 0.007$ is chosen.

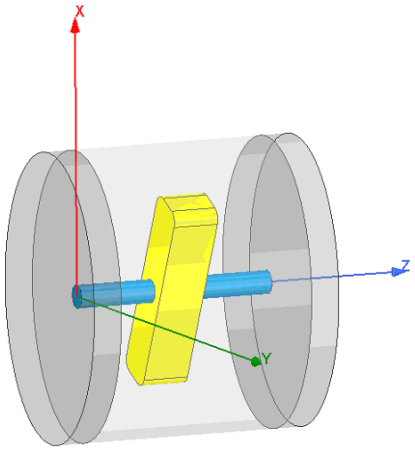

Figure 3.15: Single cavity. In it, a metallic post hold by a rod.

To measure the impact of the rod on the structure, a single resonant cavity with the rod is simulated. Figures 3.16a and 3.16b show a comparison of the structure with and without the rod. The inclusion of the rod slightly degrades the unloaded quality factor, but the response in frequency keeps being the same.

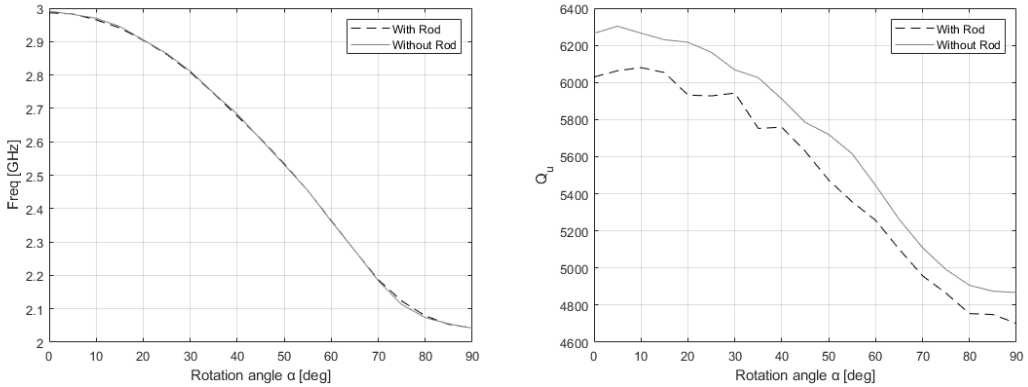

(a) Resonance frequency

(b) Unloaded Q

Figure 3.16: Impact of the rod on the resonant structure

Concerning the product of $f_r \times K_{ij}$, the addition of the rod changes the shape of the product over α. However, the previously designed irises are maintained as the impact is small.

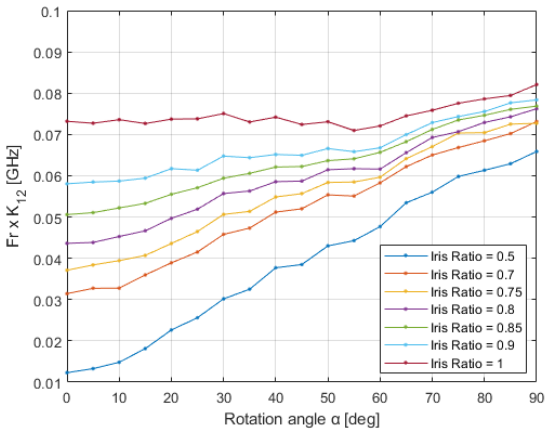

Figure 3.17: Impact of the rod - $f_r \times K_{ij}$ with different elliptic irises: axis variation with fixed major axis to 25mm

3.2.5 External Couplings

In this section, the external couplings from source to resonator and, consequently, resonator to load are analyzed. For this reason, the ports that will load the filter need to be designed. As explained in chapter 2, we will focus on the group delay method to determine the external coupling and design the input/output couplings.

A good simulation setup for the external coupling analysis is to use a cavity, with its metallic post, loaded with the input-output (I/O) port and, then, add the consecutive cavity empty with the correspondent coupling iris as figure 3.18a.

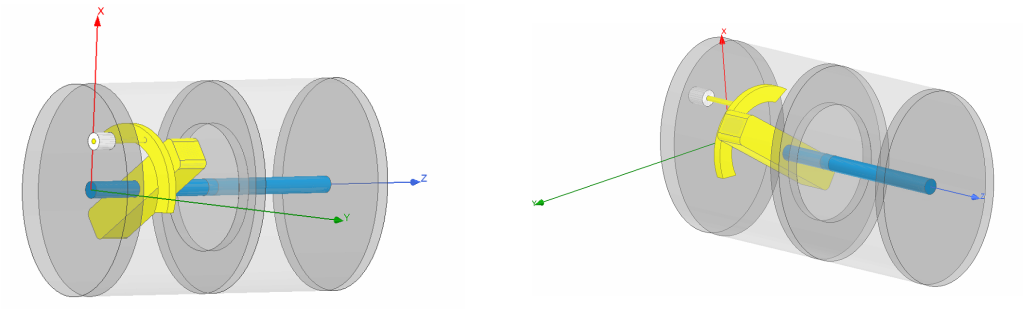

(a) View 1

(b) View 2

Figure 3.18: 3D model of the cavities with the external coupling.

This setup is good enough for determining the reflection group delay. The resonance frequency is not modified because of couplings with other resonators and the environmental conditions of the post are almost the real ones of the complete filter.

For the purpose of maintaining a constant bandwidth and acceptable return loss in the whole tuning

range, it is important to have a constant peak reflection group delay as equations 2.5 and 2.6 suggest. In the proposed design, a shaped metallic probe is utilized to realize the required I/O coupling. This probe is connected to an SMA connector.
The shaped probe has three degrees of freedom, the gap, the position and the probe angle. In order to ease the design of this probe, the gap and the position of the feeding point are modified until a desired reflection group delay peak is obtained at the center band of the tuning range. Then, the probe is extended in both sides to realize the desired and constant I/O coupling over the tuning range.

If equation 2.6 is applied, for a fractional bandwidth of a 4% around the 2.5GHz, the required Q_e is 28.33, resulting in an approximately 7.22 nanoseconds of reflection group delay. The values of the lowpass immitances are extracted from the coupling matrix defined in Appendix A.1, using equation 2.8. Now, the I/O probes are placed in a point where the desired value of group delay is achieved and, then, they are extended in both ways to achieve such Q_e in the whole range.

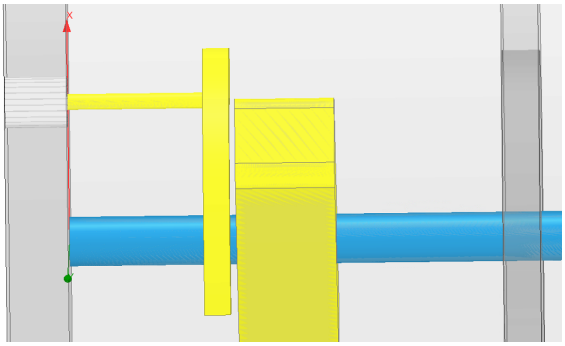

Figure 3.19: Cross section of the external coupling. Gap between post and probe.

10.9 millimeters separates the shaped probe from the external wall of the cavity and 0.5mm separates the probes and the metallic post (defined as the gap). The SMA port is placed at a point defined as (12, 6) millimeter in the XY plane. As equations 2.4 and 2.6 suggest, if the peak of the group delay is constant, the quantities of Q_e and bandwidth are constant.

A roughly constant group delay of 8 nanoseconds is achieved at the center bands of the filter. Constancy is lost at the highest frequencies.

3.2.6 Filter adjustments

The addition of the external I/O shaped probe might alter the resonant cavity. The filter is synthesized and designed considering equal resonators. For this reason, modifying the structure might lead to an undesired degradation of the filter response if the resonances of the loaded and unloaded cavities are different.
The resonance frequency of the cavity loaded with the shaped I/O coupling is analyzed and compared in

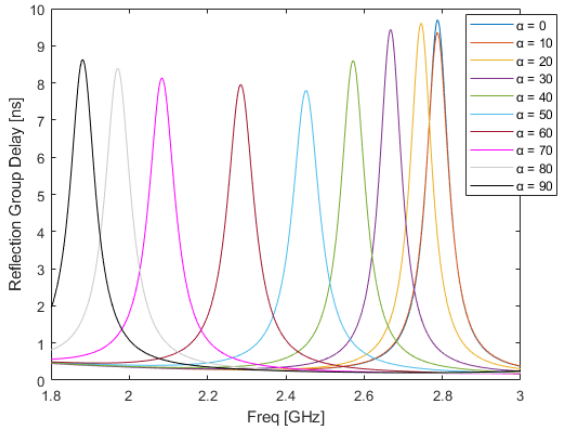

Figure 3.20: Simulated Group Delay

figure 3.21 against the cavity with a single metallic post, previously analyzed.

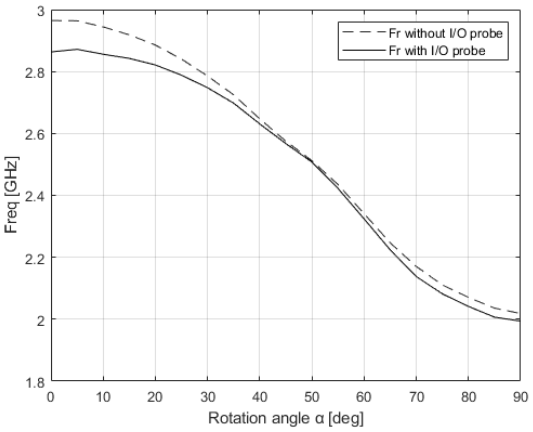

Figure 3.21: Resonance frequency comparison - Effects of the metallic shaped probe

This inclusion of the port also added a significant difference in the firsts 35 degrees. The response is quite good for the rest of angles even though it is slightly degraded at the higher ones.
To ease the comprehension of the following adjustment exercise, we will refer to the resonance frequency of the loaded cavity (with the shaped probe) as Fr_1 and to the resonance frequency of the unloaded cavity (without the shaped probe) as Fr_2.

A M5 (Metric 5) screw is placed at an angle of 15 degrees in order to absorb and correct the big differences of the highest frequencies. By reducing the gap of the post and the external wall, the resonance frequency is reduced as seen in section 3.2.2. For this reason, the screw is placed in the unloaded cavity, as it exhibits a higher resonance frequency. After several optimization exercises, best matching of frequencies is obtained when the screw is 4.1mm introduced. This screw will be considered in the fabrication step and will help the designer to correct the difference in resonances as well as the fabrication tolerances.

Once the optimal point is found, the screw is permanently fixed.

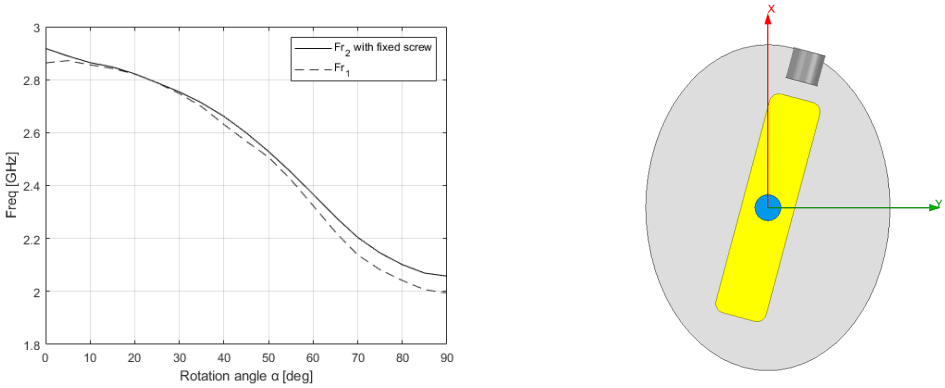

(a) Simulated Fr (b) Cavity 2 - 3D Model

Figure 3.22: Comparison of Fr_1 and Fr_2 with fixed screw in Case 2

Fr_2 is corrected for high frequencies (thus, low values of α). At lower frequencies, the difference became greater. A second M5 screw is placed in the first cavity at an angle of 55 degrees. This second screw has the task of partially absorb the impact of loading the cavity. After a parametric sweep of the screw's depth in the cavity, an optimal value of 1.5mm is found.

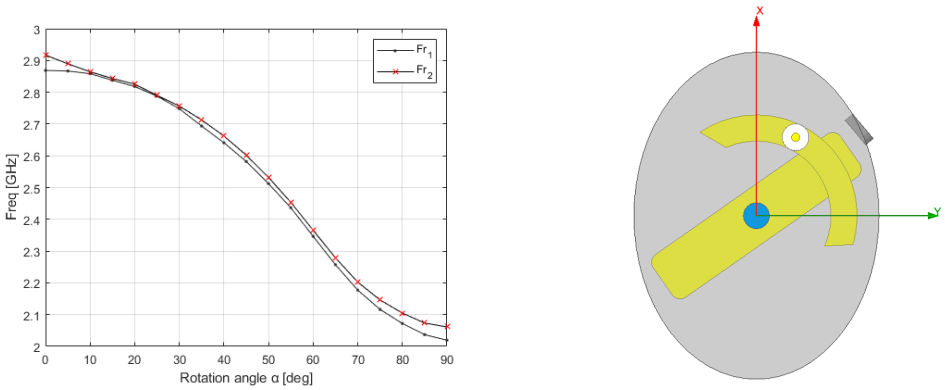

(a) Simulated Fr (b) Cavity 1 - 3D Model

Figure 3.23: Comparison of Fr_1 and Fr_2 with fixed screws in Case 1 and Case 2

The authors of [11] proposed the addition of those two fixed screws. Additionally, they considered shortening the length of the metallic posts that control Fr_2 to 34.76mm. If this shortened length is considered in our analysis, after a optimization process, a more accurate response is obtained as shown in figure 3.24.

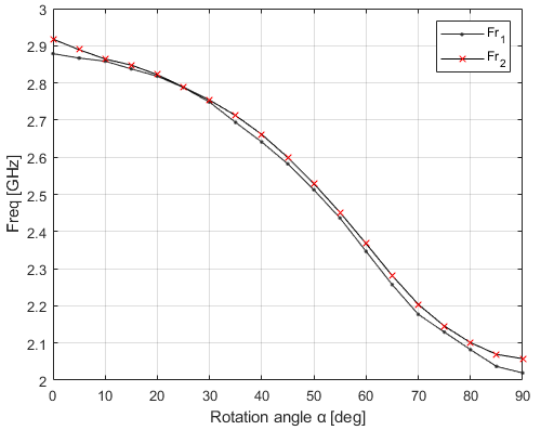

Figure 3.24: Resonance frequency comparison with fixed screws (Screw Case 1 depth = 1mm; Screw Case 2 depth = 4.3mm)

3.3 Simulated filter response

In this point, all the parts of the filter have already been meticulously designed. The filter is ready for simulation. A 3D model of a 4-order filter is shown in figure 3.25 and its dimensions are in table 3.3.

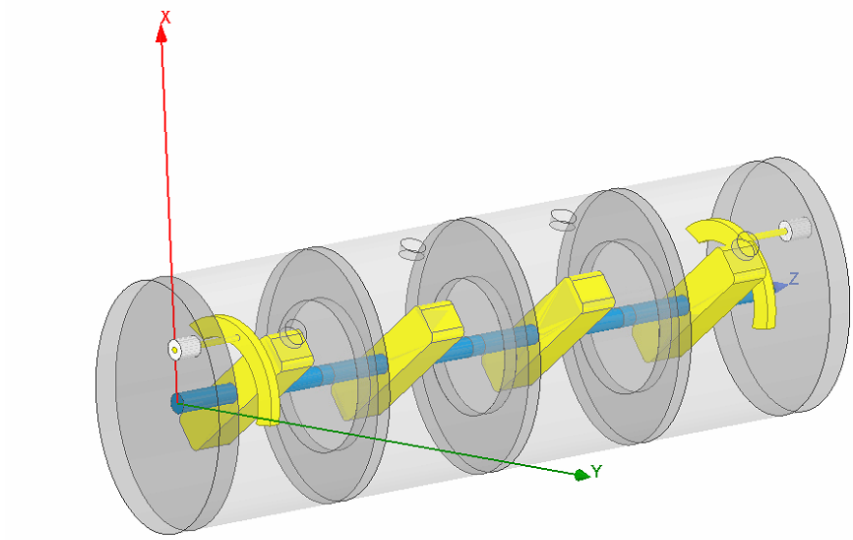

Figure 3.25: 3D Model of the entire filter

The simulated S parameters are in figure 3.26. A tuning range from 10° to 60° degree is achieved without significant degradation in the filter's response. As stated before, the best response of the rotational tuning is obtained at the central bands of the tuning range. Quantities such as group delay and the product of $F_r \times K_{ij}$ were better suited for the higher bands of the filter.

Elliptic parts	**Major Axis**	**Axes Ratio**	**Thickness**
4 Cavities	50	0.75	35
Iris 12 (= Iris 34)	30	0.85	3
Iris 23	27	0.85	3
Metallic post	**Length**	**Width**	**Thickness**
Post 1 (= Post 4)	35	8	8
Post 2 (= Post 3)	34.76	8	8
Tuning mechanism	**Diameter**		
Rod	4		
Input/Output Probe	**Angle**	**Gap**	**Thickness**
2 Shaped Probes	138	0.5	2.1
Fixed Screws	**Location**	**Depth**	**Diameter**
Screw 1 (= Screw 4)	50	1	5
Screw 2 (= Screw 3)	15	4.3	5

Table 3.3: Dimensions of the designed tunable filter (dimensions in "mm", angles in "deg")

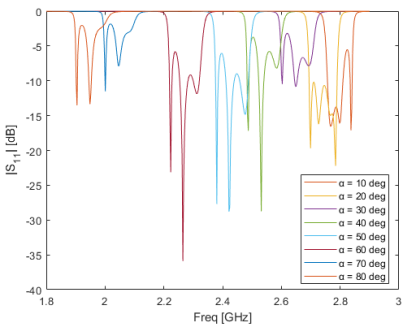

(a) Simulated S11 - Magnitude

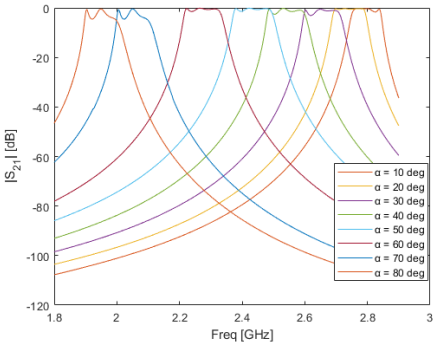

(b) Simulated S21 - Magnitude

Figure 3.26: Filter simulation - S parameters

An absolute bandwidth and insertion loss with minimum variations are obtained as figures 3.27a and 3.27b demonstrates. Bandwidth is around the 100 MHz while insertion loss do not overpass the 0.5dB, measured at the reflection zeros.

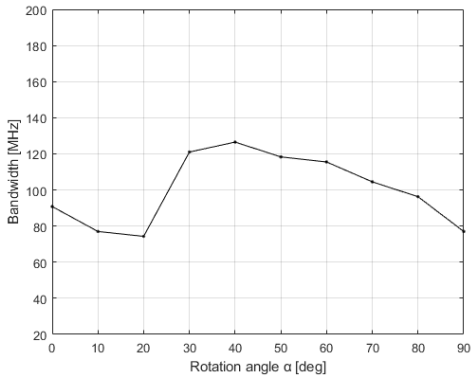

(a) Simulated Absolute Bandwidth

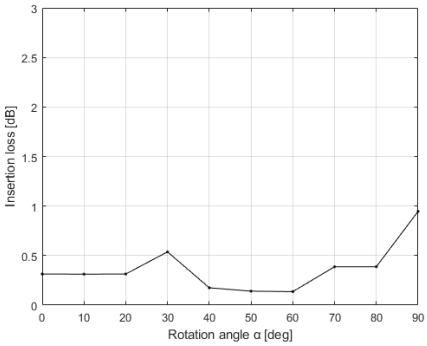

(b) Simulated Insertion Loss

Figure 3.27: Filter simulation - Bandwidth and insertion loss

Chapter 4

Measurements of the High-Q Tunable Filter under study

In this chapter, the fabrication, assembly and measurements on the proposed tunable filter are realized. At the beginning of the chapter, the fabrication and assembly are covered. Lately, the measurements of the real filter and its constitutive parts are carried out. Finally, the actual response of the whole assembled filter is measured.

4.1 Fabrication and assembly

The fabrication of the constitutive parts of the elliptical filter was mainly done outside UAB. The companies in charge of that were *Ferreteria Maranges S.A.* and its provider *Mecanytec S.L.*. They were in charge of all the conductor pieces of the filter, excluding the input and output connector ports. The dielectric rod was fabricated in the UAB. Several options appeared for the rod, however the most consistent option was to use a PVC rod.
In appendix A.3, the final drawings for fabrication are shown. In order to ease the assembly, the filter is designed by parts. Ears are given to the biggest pieces, all of which constitute the filter internal and external walls —— mainly cavities and irises —— in order to allow the union of them by means of screws.

4.1.1 Materials

A good option for prototyping is the use of aluminum as conductor. Lots of different alloys of aluminum exist and almost all of them have good electrical characteristics with low cost as compared with other conductors such as copper or gold.
For our filter prototype, we decided to use the alloy EN AW-6082 of aluminum for its conductivity

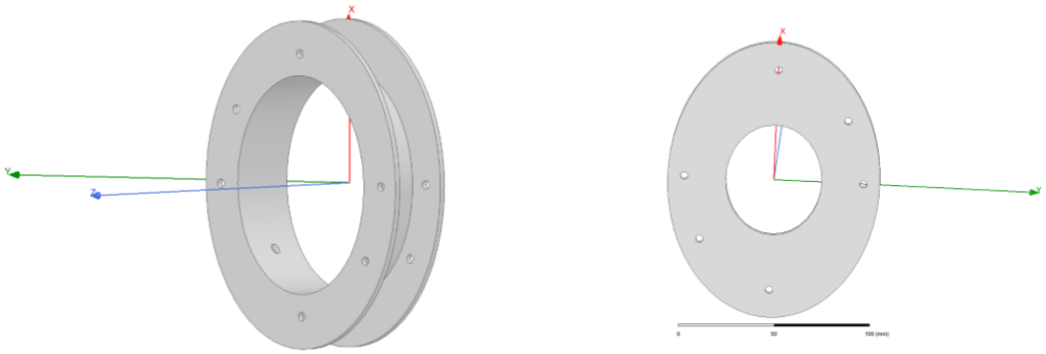

(a) Case (b) Iris

Figure 4.1: Example of fabricated pieces

properties. This alloy is one of the most conductive aluminums that our provider (*Broncesval S.L.*) had in catalog.

EN AW-6082		
Specific Weight $[g/cm^3]$	Electric Resistivity $[\mu\Omega \cdot m]$	Electric conductivity [% IACS]
2.7	37	48.6

Table 4.1: Aluminum EN AW-6082 properties

For the dielectric, different options were available. The rod goal is to hold the resonators aligned with minimum impact in the electromagnetic properties. To accomplish the condition of being invisible to the waves as much as possible, a dielectric with low relative permittivity ϵ_r and minimum losses is needed. However, the rod diameter is 4 millimeter, being a very thin rod. To avoid that the rod bends with the minimum force, a compact and rigid material is necessary. Our final chose was a rigid Polyvinyl Chloride (PVC) rod.

Rigid PVC	
Electrical Properties	
Dielectric Permittivity ϵ_r	Tangent loss $tan\delta$
3-4	0.006-0.02

Table 4.2: Rigid PVC - Electrical properties

The SMA connectors chosen were gold-made following the specifications of the standard MIL-STD-348A [15].

Rigid PVC	
Mechanical Properties	
Strength at Break (Tensile) [MPa]	Strength at Yield (Tensile) [MPa]
35-60	35-50

Table 4.3: Rigid PVC - Mechanical properties

4.2 Measurements and adjustments

In this stage of the project, the final and actual response of the filter is shown. As the filter structure is complex, the assembly of it must be done carefully. For this reason, the mounting process is done following the same procedures than in the previous chapter of simulations. First, the sweep in frequency of a single unloaded resonator and the couplings are proved. Then, the external coupling probes are mounted in such a way that the desired group delay is obtained over the whole range. Finally, the whole filter is measured.

4.2.1 Measurements of the Resonance Frequency

For this case, the measurement setup is quite similar than in chapter 3 of simulations. One single cavity with one aluminum post inside. However, in order to measure the eigenmodes of the structure is necessary the addition of ports, as a Vector Network Analyzer is used. To be able to minimize the impact of the ports, ports of short probe are used. Those ports are good enough to measure the resonance frequency minimizing the impact of them in the structure.

Figure 4.2: Input probe for eigenmodes analysis - 5.7mm

In this case, the probes are introduced 5.7mm, instead of the 10.9mm that the shaped probe require. Each port do not face the other port in order to avoid as much as we can the loading effect of the ports. These ports must excite the desired TE mode, but avoiding loading the metallic post.

Figure 4.3: One single cavity

What we should expect to see in the display of the measurement instrument is a resonance at a determined frequency (an S21 maxima at the resonance frequency). If we extract and post-process this measurement in Matlab, this is the sweep in frequency obtained.

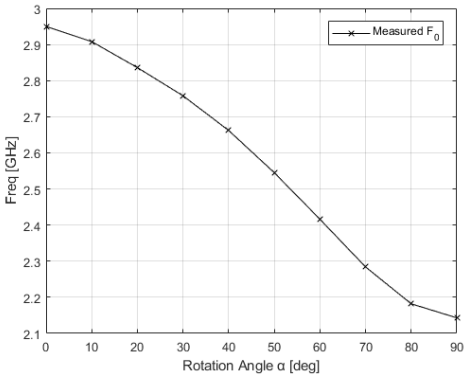

Figure 4.4: Measured Resonance Frequency

The rotational tuning works fine. The sweep in frequency is achieved. A thinner frequency tuning range is measured as compared with the simulations.

4.2.2 Measurements of the Interresonator Couplings

The setup for the measurement of the coupling effect is the same than in previous chapter. Two cavities with their metallic posts inside and the coupling iris under study between them. Following the same procedure as in previous section for the eigenmode analysis, the shortened probes of figure 4.2 are used.

As two resonant cavities are coupled, in the display of the measurement instrument two resonances are expected to appear at two different frequencies (two S21 maximas). Those resonances are the conse-

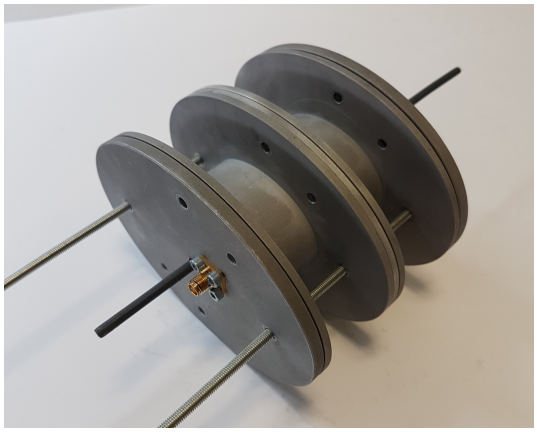

(a) Setup for the interresonator couplings measurement

(b) Iris 23

Figure 4.5: Coupling measurement. Setup and example of coupling iris

quence of the interresonator couplings, as stated in chapter 2. After extracting and post-processing these measurements in Matlab, these are the obtained results for both coupling irises (Iris12 and Iris23).

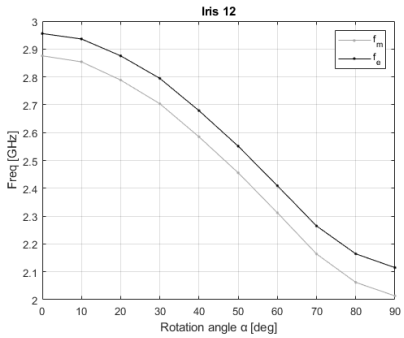

(a) Iris 12 (= Iris 34)

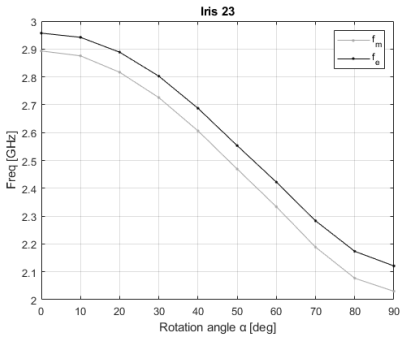

(b) Iris 23

Figure 4.6: Couplings measurements

The sweep in frequency of both resonances is achieved with good performance and maintaining an approximately constant distance between resonances. The designed coupling irises work respecting the rotational tuning, thanks to the elliptic shape given to those irises.
Applying expression 2.2, the physical coupling could be obtained and, therefore, the product of $f_r \times K_{ij}$. As we have stated in previous chapter, if this product is maintained constant over the tuning range, the bandwidth will also remain constant.

However, as stated in chapter 3, the addition of the rod makes that the product of $f_r \times K_{ij}$ has a positive slope while increasing α.

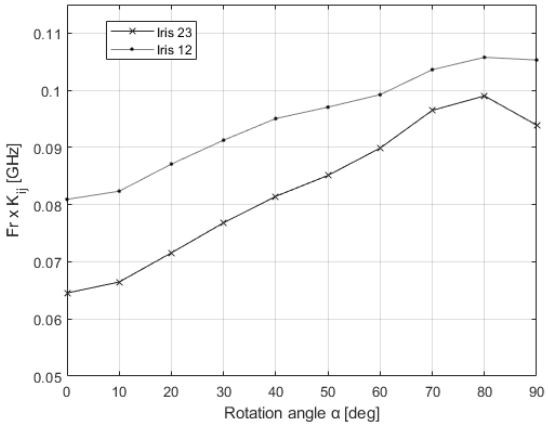

Figure 4.7: Product of $f_r \times K_{ij}$

4.2.3 External coupling assembly and measurements

The montage of the external probe is a critical point in our structure. This circular shaped probe is almost a floating element that should be strictly fixed at the position where the group delay stays constant over the tuning range. If the probe is not correctly placed or aligned, the coupling for some rotation angles might be bigger or shorter, making impossible to ensure a constant external coupling. For this reason, several trials were necessary to find a position where the group delay remained constant.

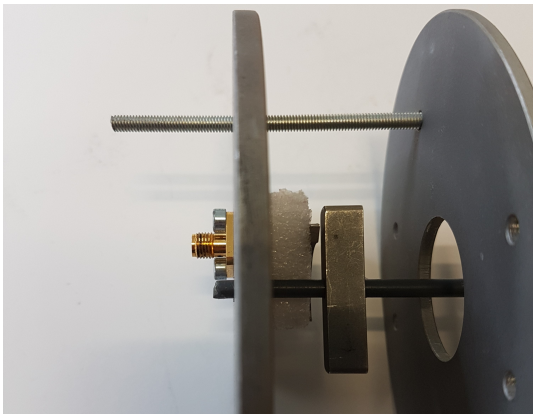

Figure 4.8: Probe position and support

The obtained results of group delay are shown in figure 4.9.

A group delay of approximately 9ns is achieved at the central points of the band. However, at the ends the difference is more relevant.

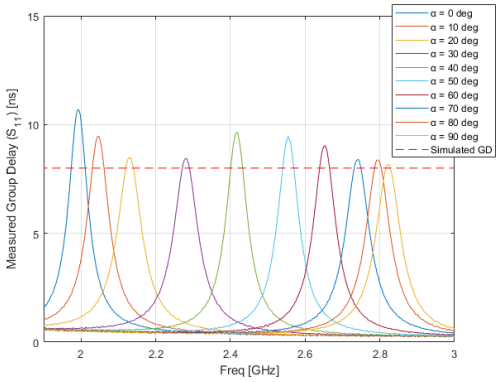

Figure 4.9: Measured group delay over the whole tuning range

4.2.4 Measurement and performance of the assembled filter

The assembly of the complete filter must be done carefully as the minimum movement or displacement of a single element might cause that the filter do not work as expected. A single deviation might do that measurements are not repeatable.

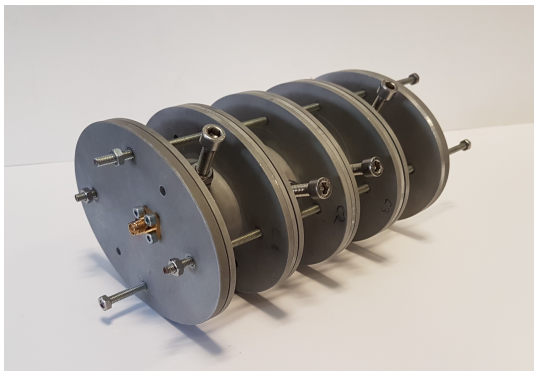

Figure 4.10: Complete assembled filter

In figure 4.11 the obtained results of a whole filter run are shown.

A tuning range from 2GHz to 2.6GHz is achieved without significant degradation of the filter response. An absolute bandwidth and insertion loss with minimum variations are obtained as figures 4.12a and 4.12b demonstrates.

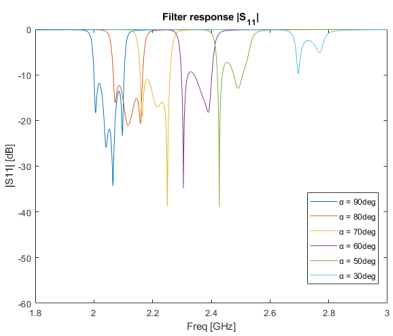

(a) Measured S11 - Magnitude

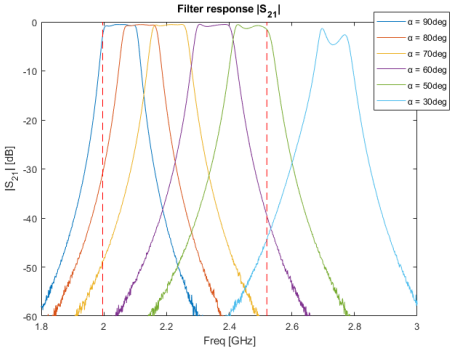

(b) Measured S21 - Magnitude

Figure 4.11: Filter response - S parameters

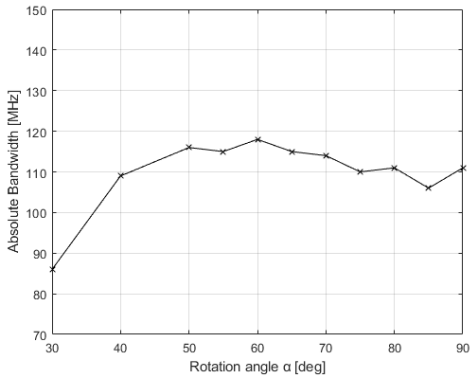

(a) Measured Absolute Bandwidth

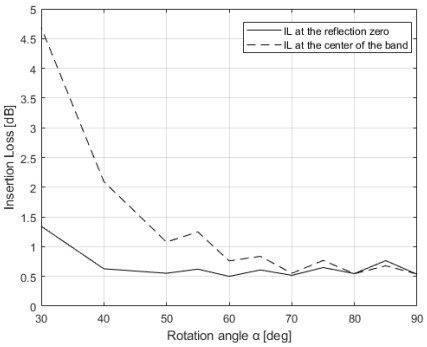

(b) Measured Insertion Loss

Figure 4.12: Filter response - Bandwidth and insertion loss

Fine measurements could not be done because of the extraordinary circumstances of the ending part of the course. Fixed screws adjusments were not performed. So, improvements of the filter's response are expected once the elements get finely placed.

Chapter 5

Conclusions

In this work the general design steps for a tunable filter have been presented. Specifically, a three dimensional filter is replicated and extensively analyzed with the big advantage of having a single tuning element. The remarkable need of having reconfigurable technology in a connected world that continuously evolves mixed with the simplicity of the tuning mechanism that is presented make the project attractive.

Thanks to the electromagnetic simulation software, High-Frequency Structure Simulator (HFSS), a deep analysis has been done in this thesis for the tuning idea presented in [2]. A replica in HFSS is designed, following the design procedures of tunable filters. Things like the general resonant structure, the interresonator couplings and the external I/O coupling could be designed in detail. Moreover, the impact of loading the cavity have been studied and corrected by means of fixed screws. A tuning range of around 750MHz is achieved with minimun variations in bandwidth and insertion loss in the frequency band of 2.5GHz.

A similar replica of the proposed filter is manufactured and measured in this work. Notice that some deviations are found due to the materials used and the degrees of freedom that the prototype of [2] presented. A tunning range of 550MHz is achieved with minimum variations in bandwidth and insertion loss. However, the simulated filter response could not be achieved for the manufactured prototype. The filter could not be finely adjusted due to the extraordinary circumstances that this course have had.

Objectives could be achieved, as the prototype tunable filter is designed, studied and measured. The theory behind the design of a tunable filter is followed and studied, considering all the quantities that leads to have a high performance 3D filter over the whole tuning range. The results of the tunable filter of single tuning element are great, taking into account that tuning screws were not placed when measuring the filter.

As seen throughout this thesis, the world of reconfigurable filters is still a challenging topic. In terms of future lines, different reconfigurable filters of single tuning element could be a general and interesting

topic for research. Concerning the proposed filter, other prototypes of higher order or multiplexers might be interesting to design and manufacture. Different interresonator couplings could be considered and analyzed as well as the shape and position of the I/O coupling could be modified taking into account the periodicity in frequency that the filter could give (notice that only 90 degree out of 360 are used). Also, a system for controlling the rotational tuning could be added.

Additionally, a big counterpart of three-dimensional filters is the size and weight of the RF component. Despite of the fact that on-satellite systems can sacrifice size as the expense of high performance and Q, the size is still a drawback to correct. For this reason, an interesting topic to study and research are miniaturization techniques for the proposed filter.

Appendix A

A.1 Coupling Matrix of a 4-pole Chebyshev function considering RL = 16dB

For an all pole Chebyshev function of fourth degree with RL = 16dB and following an in-line topology requiring only magnetic couplings, the resulting coupling matrix is

$$\mathbf{M} = \begin{pmatrix} 0 & 0.9392 & 0 & 0 & 0 & 0 \\ 0.9392 & 0 & 0.8221 & 0 & 0 & 0 \\ 0 & 0.8221 & 0 & 0.6530 & 0 & 0 \\ 0 & 0 & 0.6530 & 0 & 0.8221 & 0 \\ 0 & 0 & 0 & 0.8221 & 0 & 0.9392 \\ 0 & 0 & 0 & 0 & 0.9392 & 0 \end{pmatrix} \tag{A.1}$$

This is the coupling matrix considered througout the design of the tunable filter with single tuning element. This matrix is synthesized following a recursive method from the reflection and transmission polynomials explained in [1]. For example, the element M_{01} (also typically denoted as M_{s1}) is 0.9392, quantifying the necessary coupling between source to resonator 1. The element M_{34} is 0.8221, quantifying the necessary coupling between resonator 3 and 4.

A.2 Modal distribution of a single resonant cavity

Given the following elliptical structure with a major axis of 50mm and an axis ratio of 0.75 and a metallic post of dimensions 35x8x8 mm^3

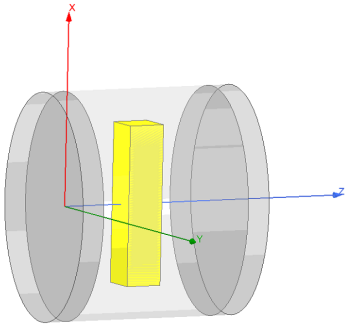

Figure A.1: 3D model of the resonant cavity in HFSS

The first four modes that can be excited are

Allowed modes within 1GHz and 6GHz		
Eigenmode	Frequency [GHz]	Q_u
Mode 1	2.911	6156.15
Mode 2	4.968	9404.81
Mode 3	5.037	9024.84
Mode 4	5.893	8574.11

Table A.1: First four modes with its Q_u ($\alpha = 0$)

The first mode (TE Mode) is deeply analyzed in chapter 3. The second, third and fourth mode field distributions are

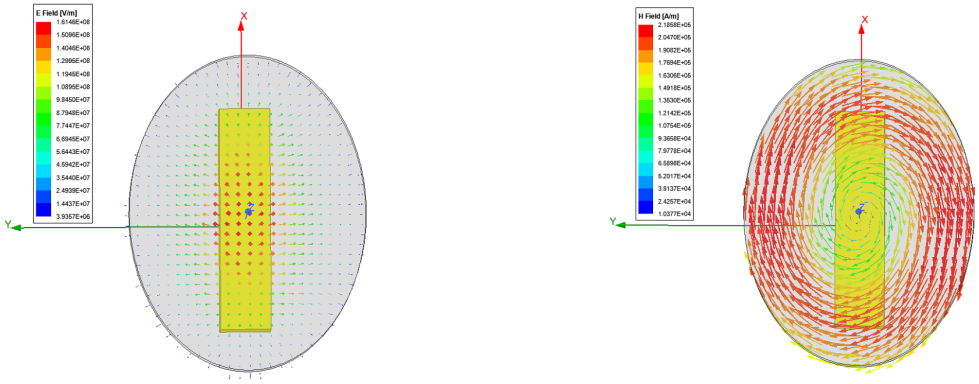

(a) Electric field distribution (b) Magnetic field distribution

Figure A.2: Fields distribution of mode 2 at $\alpha = 0$ - TM Mode

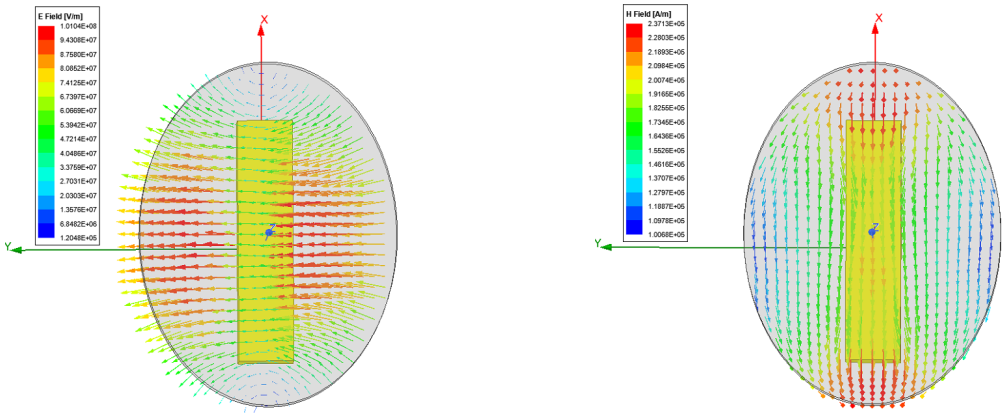

(a) Electric field distribution (b) Magnetic field distribution

Figure A.3: Fields distribution of mode 3 at $\alpha = 0$ - TE Mode

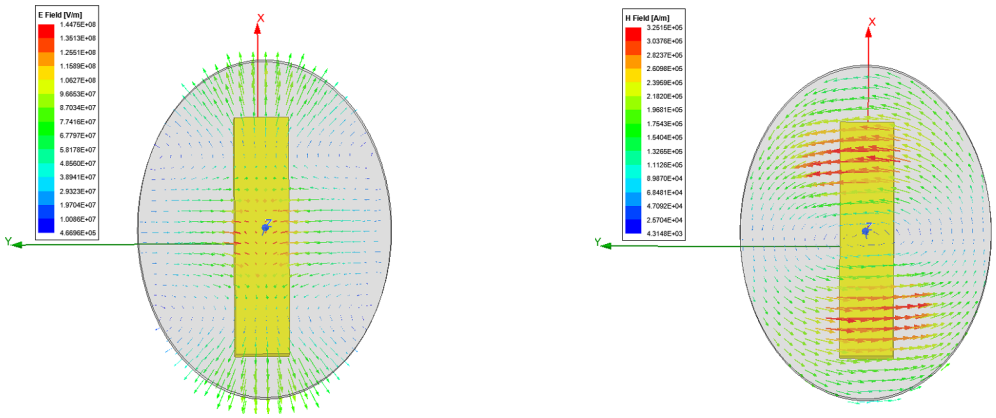

(a) Electric field distribution (b) Magnetic field distribution

Figure A.4: Fields distribution of mode 4 at $\alpha = 0$ - TM Mode

A.3 Filter manufacturing - Elements and dimensions

Parts of the manufactured filter.

Element Name	Total units
Res 1	2
Res 2	2
Case 1	2
Case 2	2
Iris 12	2
Iris 23	1
Shaped Probe	2
Plate 1	1
Plate 2	1

Table A.2: Manufactured parts

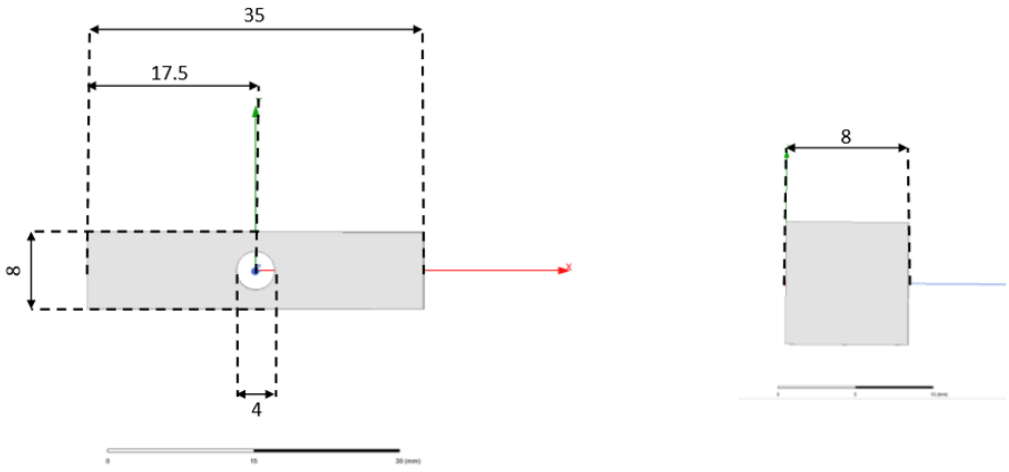

Figure A.5: Res1 - Metallic post 1 and 4 (units in millimeters)

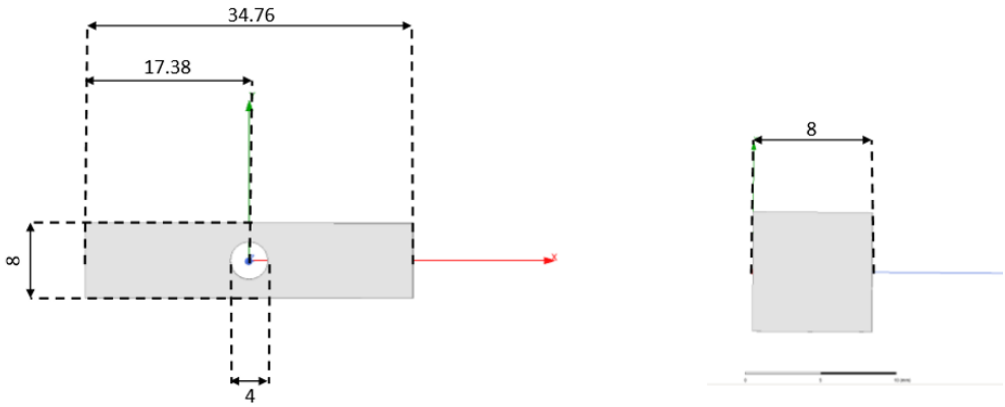

Figure A.6: Res2 - Metallic post 2 and 3 (units in millimeters)

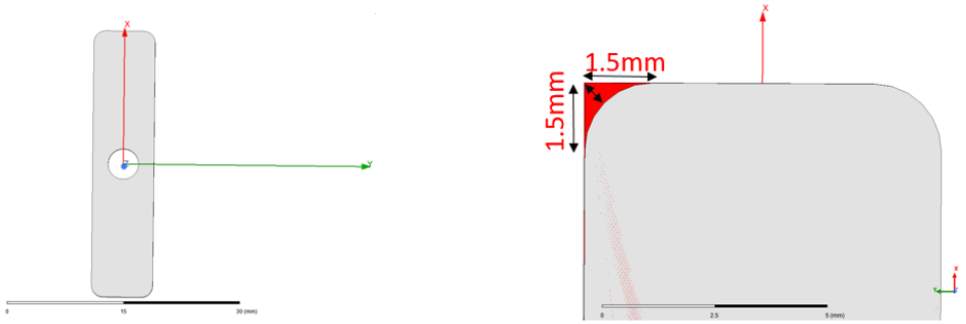

Figure A.7: Res1 and Res2 - Detail (units in millimeters)

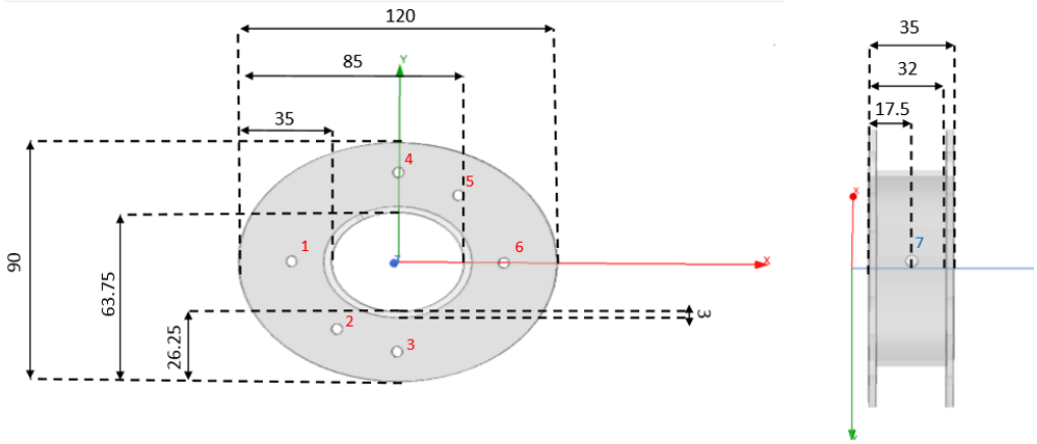

Figure A.8: Case 1 - Cavity 1 and 4 (units in millimeters)

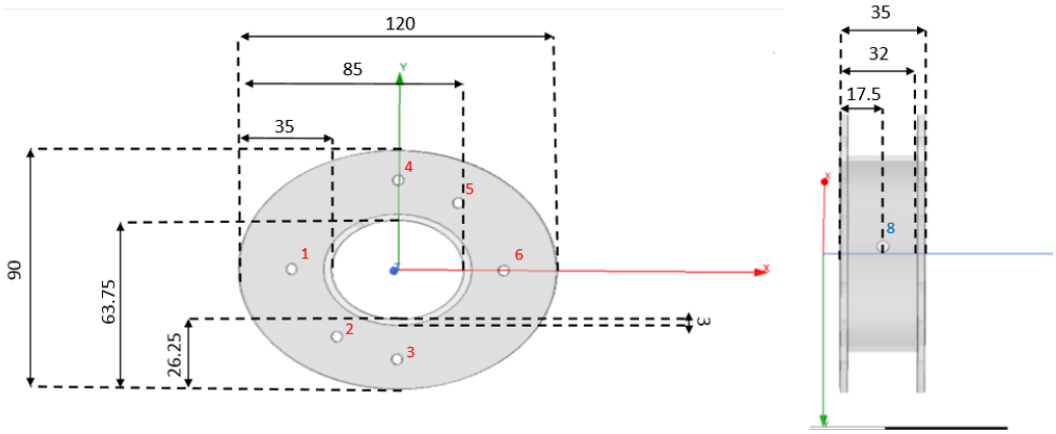

Figure A.9: Case 2 - Cavity 2 and 3 (units in millimeters)

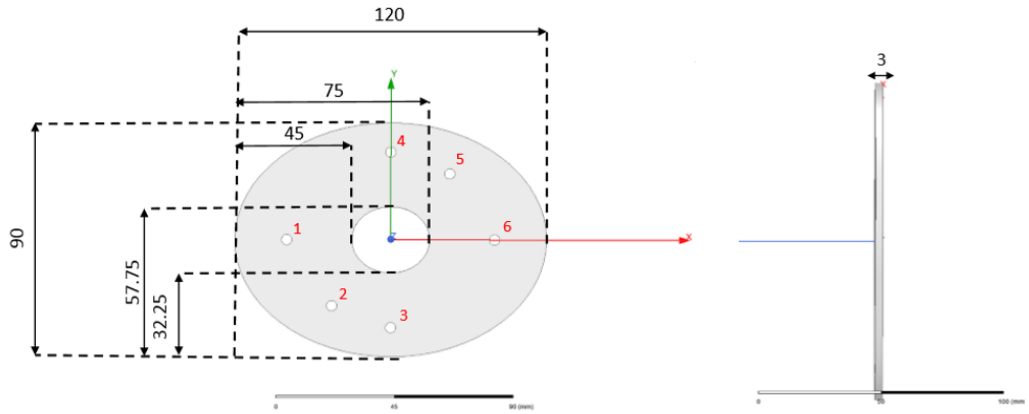

Figure A.10: Iris 12 and Iris 34 (units in millimeters)

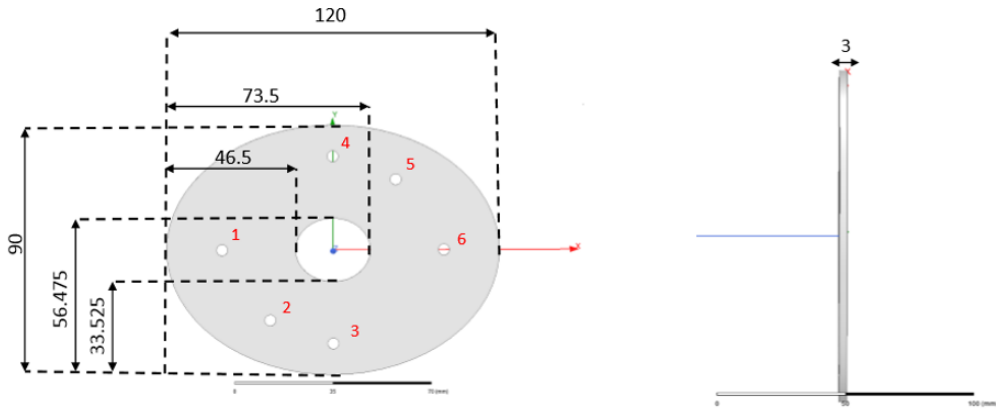

Figure A.11: Iris 23 (units in millimeters)

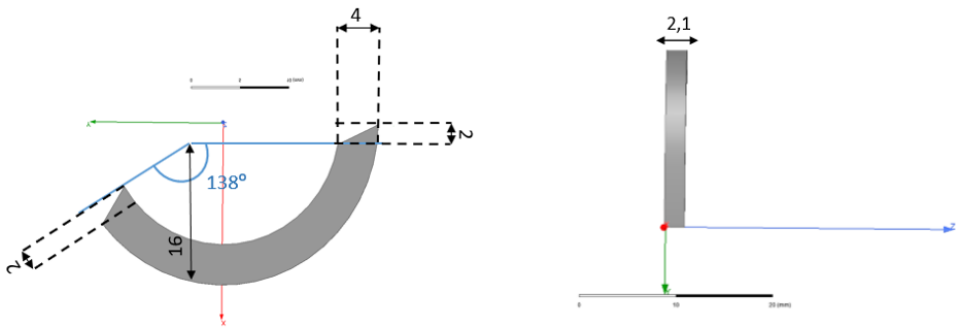

Figure A.12: Shaped Probe 1 and 2 (units in millimeters)

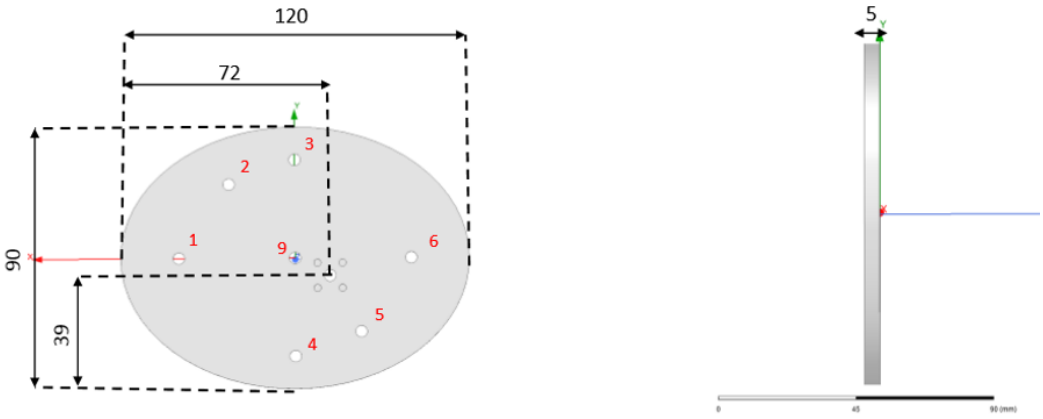

Figure A.13: Plate 1 (units in millimeters)

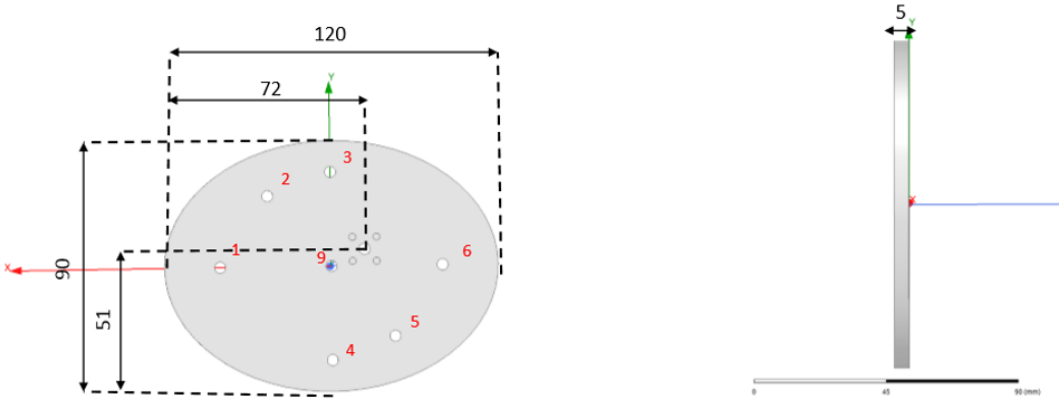

Figure A.14: Plate 2 (units in millimeters)

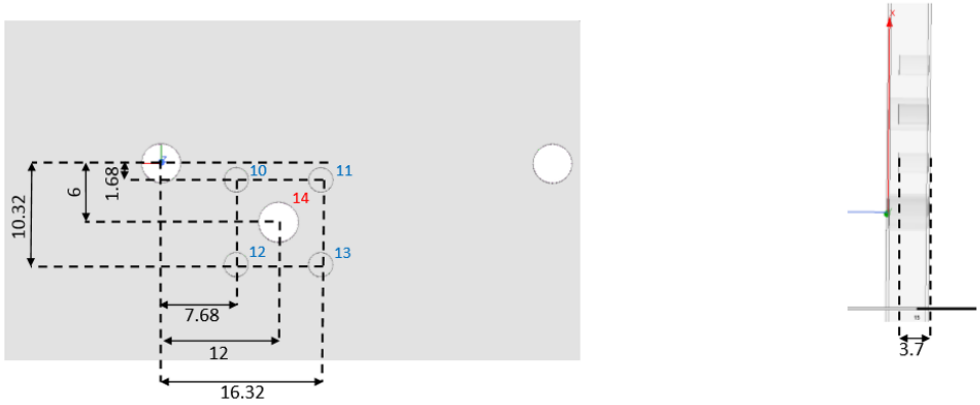

Figure A.15: Plate 1 and plate 2 - Detail (units in millimeters)

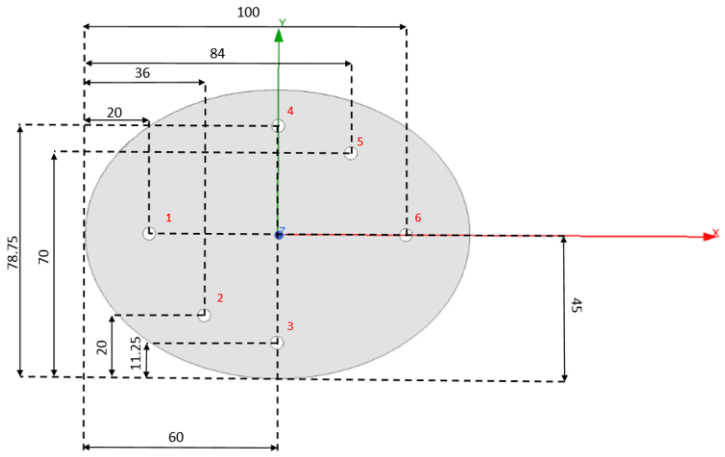

Figure A.16: Detailed position of common holes 1, 2, 3, 4, 5 and 6 (units in millimeters)

Hole number	**Diameter [mm]**	**Description**
1, 2, 3, 4, 5, 6	4	Common holes for assembling the filter
7	5	Threaded hole placed at 40° from axis y
8	5	Threaded hole placed at 75° from axis y
9	4	-
10, 11, 12, 13	2.5	Threaded hole; 3.7mm depth
14	4.1	-
15, 16, 17, 18	2.5	Threaded hole; 3.7mm depth
19	4.1	-

Table A.3: List of holes and description

Bibliography

[1] R. J. Cameron, C. M. Kudsia, and R. R. Mansour, *Microwave Filters for Communication Systems*. John Wiley & Sons, 2018.

[2] G. B. and R. R. Mansour, "A tunable coaxial filter with minimum variations in absolute bandwidth and q using a single tuning element," in *2019 IEEE MTT-S International Microwave Symposium (IMS)*. IEEE, jun 2019.

[3] M. G. C. Branco and A. da Rocha Gomes, "Satellite communication challenges in a fully interconnected world," in *2017 SBMO/IEEE MTT-S International Microwave and Optoelectronics Conference (IMOC)*. IEEE, aug 2017.

[4] D. M. Pozar, *Microwave Engineering*. John Wiley & Sons Inc, 2011.

[5] R. Gomez-Garcia, M.-A. Sanchez-Soriano, K.-W. Tam, and Q. Xue, "Flexible filters: Reconfigurable-bandwidth bandpass planar filters with ultralarge tuning ratio," *IEEE Microwave Magazine*, vol. 15, no. 5, pp. 43–54, jul 2014.

[6] K. Nishikawa and M. Muraguchi, "Dual-mode frequency tunable planar filter design with capacitive coupling technique," in *2018 IEEE International Symposium on Radio-Frequency Integration Technology (RFIT)*. IEEE, aug 2018.

[7] R. R. Mansour, F. Huang, S. Fouladi, W. D. Yan, and M. Nasr, "High-q tunable filters: Challenges and potential," *IEEE Microwave Magazine*, vol. 15, no. 5, pp. 70–82, jul 2014.

[8] M. S. Anwar and H. R. Dhanyal, "Design of s-band combline coaxial cavity bandpass filter," in *2018 15th International Bhurban Conference on Applied Sciences and Technology (IBCAST)*. IEEE, jan 2018.

[9] W. D. Yan and R. R. Mansour, "Tunable dielectric resonator bandpass filter with embedded MEMS tuning elements," *IEEE Transactions on Microwave Theory and Techniques*, vol. 55, no. 1, pp. 154–160, jan 2007.

[10] S. Fouladi, F. Huang, W. D. Yan, and R. R. Mansour, "High-q narrowband tunable combline bandpass filters using MEMS capacitor banks and piezomotors," *IEEE Transactions on Microwave Theory and Techniques*, vol. 61, no. 1, pp. 393–402, jan 2013.

[11] G. Basavarajappa and R. R. Mansour, "Design methodology of a high-q tunable coaxial filter and diplexer," *IEEE Transactions on Microwave Theory and Techniques*, vol. 67, no. 12, pp. 5005–5015, dec 2019.

[12] F. Huang, "High-q tunable lters," Ph.D. dissertation, University of Waterloo, Waterloo, Ontario, Canada, 2012.

[13] S.-J. Zhang and Y.-C. Shen, "Eigenmode sequence for an elliptical waveguide with arbitrary ellipticity," *IEEE Transactions on Microwave Theory and Techniques*, vol. 43, no. 1, pp. 227–230, 1995.

[14] J. Kretzschmar, "Field configuration of the TMc01 mode in an elliptical waveguide," *Proceedings of the Institution of Electrical Engineers*, vol. 118, no. 9, p. 1187, 1971.

[15] U. D. of Defense, *Radio Frequency Connector interfaces for MIL-C-3643, MIL-C-3650, MIL-C-3655, MIL-C-25516,MIL-C-26637, MIL-C-39012, MIL-C-49142,MIL-A-55339, MIL-C-83517.*